Cell Host & Microbe, Volume *15*

Supplemental Information

Mechanisms Underlying Robustness and Tunability in a Plant Immune Signaling Network

Yungil Kim, Kenichi Tsuda, Daisuke Igarashi, Rachel A. Hillmer, Hitoshi Sakakibara, Chad L. Myers, and Fumiaki Katagiri

SUPPLEMENTAL EXPERIMENTAL PROCEDURES

Overview of the modeling approach

Our network model consists of four layers: a top input layer having three MAMP nodes (flg22, elf18, and chitosan), two signaling layers representing early and late states of four sectors, jasmonate (JA), ethylene (ET), PAD4, and salicylate (SA), a bottom output layer indicating the immunity levels against two bacterial strains, *Pto* and *Pma* (Figure 1). After normalization and preprocessing of expression levels of four sector marker genes which define the sector activities (Figures S1B-D), we fitted multiple regression models using L1-norm regularization (Lasso) (Friedman et al., 2010) (see Figure S1E and S1F for the starting model structures and the final models, respectively). The modeling approach was designed to overcome several limitations of conventional modeling approaches such as Bayesian network (Koller and Friedman, 2009) (Figure S2A). Our models were configured to predict the activity levels of four sectors and the immunity levels against two bacterial strains based on observations across four treatments including mock, two time points and 16 combinatorial genotypes. The predictive performance of the models was evaluated using a bootstrapping aggregation, which revealed high accuracy in predicting both the sector activities and immunity levels (Figures 2B and 2C). Mechanistic interpretation of the models was then accomplished through analysis of network activity maps, which allowed visualization of signal flows in the network across the combinatorial genotypes upon particular MAMP treatments (Figure S5).

Generation and preprocessing of data

Chemicals

Flg22 and elf18 peptides were purchased from EZBiolab Inc. (Westfield, IN, USA), and chitosan was purchased from SIGMA (C3646; St. Louis, MO, USA).

Selection of the sector marker genes and the normalization gene

The mRNA levels of the marker genes, At3g50280, At2g41230, At5g46960, and At2g14610 (*PR1*), were used as proxies for the JA, ET, PAD4, and SA sector activities, respectively. Datasets used for marker gene selection were the GEO datasets GSE18978 and GSE50526. In GSE18978, expression profiles were obtained from leaves of wild-type (Col-0), *coi1-1*, *ein2-1*, *npr1-1*, *pad4-1*, and *sid2-2* plants 24 hours after *Pma* (hemibiotrophic bacterium) inoculation. In GSE50526, expression profiles were obtained from leaves of wild-type (Col-0), *dde2-2*, *ein2-1*, and *sid2-2* plants 9 and 24 hours after *Alternaria brassicicola* (necrotrophic fungus) inoculation. These datasets were generated using the same tissue used in the current study and include plant genotypes highly relevant to the current study and two pathogens of very different types. The Affymetrix ATH1 Arabidopsis whole genome array was used in generating the datasets. Log_2-transformed expression level values preprocessed by GC-RMA (Wu and Irizarry, 2004) were used in the current study. In addition, the data sources of Biotic Stress, Biotic Stress II, Chemical, and Hormone in the Arabidopsis eFP Browser (http://bar.utoronto.ca/efp/cgi-bin/efpWeb.cgi) (Winter et al., 2007) were used to check the response specificity of candidate genes.

We defined the representing points of the JA, ET, and SA sectors as the respective hormone levels and selected sector marker genes that likely represent the hormone levels well. For this purpose, we used the following criteria: (1) the signal-to-noise ratio in induction by pathogens is high; (2) the induction is almost completely dependent on the sector of interest (i.e., almost no induction in the mutant corresponding to the sector); (3) strong induction by

exogenous application of the corresponding hormone (ACC in case of ET); (4) the induction is highly specific to the hormone of interest. Specific selection procedures for each sector follow:

For the JA sector marker, with GSE18978 dataset: (1) (*Pma* – mock) > 0 and the associated $q < 10^{-5}$ in WT (891 genes); (2) With *Pma*, ((*coi1* – WT) < 0 and $q < 10^{-4}$) AND ($q >$ 0.2 for all (*sid2* – WT), (*npr1* – WT), (*pad4* – WT), and (*ein2* – WT)) (244 genes). Two genes, At3g50280 and At2g39050, satisfied both selection criteria (1) and (2). (3) and (4): in the eFP Browser, At3g50280 showed strong and specific induction by MeJA. At3g50280 was selected.

For selection of the ET sector marker, GSE50526 dataset generated with *A. brassicicola* (*Ab*) infection was used since *Pma* did not seem to strongly induce ET signaling. The data for 9 hpi was used. (1) (*Ab* – mock) > 0 and q < 0.005 in WT (850 genes); (2) With *Ab*, ((*ein2* – WT) < 0 and q < 0.005) AND (q > 0.3 for both (*sid2* – WT) and (dde2-WT) (89 genes). Seven genes, At5g01210, At4g12480, At4g12470, At2g47270, At2g16060, At2g41230, and At2g44080, satisfied both selection criteria (1) and (2). (3) and (4): based on strong and specific induction by ACC and delayed induction by IAA in eFP Browser, At2g41230 was selected. It is common that ET production is induced by IAA with a delay (Abeles and Rubinstein, 1964), so delayed induction of an ET sector marker by IAA was expected.

PR1 (At2g14610) is the most commonly used SA sector marker gene (Pieterse et al., 2012) *PR1* expression level measurement by the ATH1 array is not reliable, so we did not apply the ATH1 data-based gene selection with *PR1*. However, we previously compared *PR1* expression levels, measured by qRT-PCR, and SA levels under many PTI conditions in various plant genotypes and knew that the *PR1* expression level tracks the SA level very well under PTI conditions (e.g., (Tsuda et al., 2008; Wang et al., 2009)). Thus, we used *PR1* as the SA sector marker gene.

For selection of the PAD4 sector marker gene, we were not able to use criteria (3) and (4) because a measurable signal molecule representing the sector is not known. Since it is known that PAD4 is positively regulated by SA under many conditions (Jirage et al., 1999), we added a criterion related to criterion (2): (2p) the induction level is reduced by SA sector disruption, but not as much as by PAD4 sector disruption. Similarly, (3p) induction by exogenous SA application in *PAD4* wild-type plants and (4p) the induction is highly specific to SA. We noticed that the effect of *PAD4* on the majority of these genes is mainly on the basal level and that the fold-induction was not changed much in the *pad4* mutant. Such genes do not report the PAD4 sector activity correctly because the genes are still responding in the *pad4* mutant. Thus, we added a criterion to select truly *PAD4*-dependent genes: (5) the expression level after mock treatment in wild type and the expression level after pathogen treatment in the *pad4* are similar. Thus, we used criteria (1), (2), (2p), (3p), (4p), and (5) to select the PAD4 sector marker gene, and the representing point for the PAD4 sector was defined by this marker gene. Specifically, using the GSE18978 dataset: (1) (*Pma* – mock) > 0 and $q < 10^{-5}$ (891 genes); (2) With *Pma*, ((*pad4* – WT) < 0 and $q < 10^{-4}$) AND (q > 0.2 for both (*coi1* – WT) and (*ein2* – WT)) (115 genes); (2p) With *Pma*, ((*sid2* – WT) < 0 AND (*npr1* – WT) < 0 AND (*sid2* – WT) – (*pad4* – WT) > 1 AND (*npr1* – WT) – (*pad4* – WT) > 1 (233 genes); (5) |*pad4 Pma* – WT mock| - (WT *Pma* – WT mock) < -4 (4 genes). Two genes, At5g46960 and At1g33950, satisfied all selection criteria (1), (2), (2p), and (5). (3p) and (4p), in the eFP Browser, At5g46960 showed specific induction by SA. At5g46960 was selected as the PAD4 sector marker gene.

For selection of the normalization gene, both GSE18978 and GSE50526 datasets were used. The following criteria were used for selection: (1) low variation in expression levels in each dataset; (2) no significant difference in expression level between the sector mutants and

wild type plants during pathogen infection; (3) small difference in the expression level between two experiments; (4) the mean expression level value is not very high; (5) the expression level is stable after many different pathogen-related or hormone-related treatments. Criterion (4) was included for three reasons. First, the normal hybridization conditions for Affymetrix arrays result in having the hybridization signals for highly expressed genes outside the linear range, which artificially makes expression of highly expressed genes appear more stable than it actually is. Second, using quantile normalization, hybridization signals for highly expressed genes could be highly skewed as they fall into the upper tail of the distribution, which might artificially make expression of highly expressed genes appear more stable as well. Third, quantitation by qRT-PCR is more accurate when the expression level of the normalization gene is closer to the expression level of the gene of interest. Criterion (4) excluded several conventional normalization genes. Specifically, (1) sd < 0.3 and max – min < 1.2 in each dataset (351 genes); (2) $q > 0.1$ in all (mutant – WT) in both datasets (1942 genes); (3) the mean difference between two datasets < 0.2 (1582 genes); (4) mean expression level value < 10 (10533 genes). This selection yielded 21 candidate genes. (5) based on the eFP Browser data, four genes, At4g29480, At2g30260, At3g07170, and At5g11980, were selected from the 21 genes. Among the four, At4g29480 was arbitrarily chosen as the normalization gene.

Figure S1A shows the mRNA levels of the sector marker genes, in the $\log_2$-scale relative to the normalization gene, across the treatment:genotype:time combinations. For the ET, PAD4, and SA sector marker genes, it is clear that (1) the marker gene mRNA levels are induced by MAMP treatments and (2) the induced mRNA levels are almost completely dependent on the respective sector.

Experimental design

One experimental set for the sector marker gene expression level measurement consisted of 16 or 17 genotypes (the latter of which included *fls2* in the case of flg22 treatment) with one treatment. Two ft x 1 ft flats, each of which contained eight 6 inch x 6 inch pots, were used for growing Arabidopsis plants. Two adjacent pots (a pot pair), in which the positions of 16 or 17 individual plants (one individual per genotype) were randomized, were randomly assigned to each time point. Three well-expanded leaves per individual plant were used, and leaf samples from four experimental sets were pooled for one biological replicate. Three biological replicates were made. In the case of the immunity level measurement, pot pairs were used similarly, and two leaves of each individual plant in each pot pair were used to generate a single bacterial count observation.

Measurement of the sector marker gene expression levels

Three well-expanded leaves per plant were infiltrated with mock (H_2O), 1 μM flg22, 1 μM elf18, or 100 μg/ml chitosan using a needleless syringe. At 3 or 9 hpt treated leaves were harvested and flash frozen in liquid N_2 for RNA extraction later. Different individual plants were used for different time points because excision of some leaves at 3 hpt would affect the response in other leaves of the same individual at 9 hpt. Leaves from two to four individual plants were pooled for each biological sample. Total RNA was extracted from the tissue and subjected to quantitation by quantitative reverse transcription PCR (qRT-PCR) as previously described (Tsuda et al., 2012). The obtained C_t value was used as raw data for the sector marker gene expression level (Data S1). Measurements were made in three independent experiments; these are the three biological replicates.

Measurement of MAMP-induced immunity levels

Two well-expanded leaves per plant were infiltrated with with mock (H_2O), 1 μM flg22, 1 μM elf18, or 100 μg/ml chitosan using a needleless syringe. At 24 hpt, after mock or elicitor treatment, the same leaves were infiltrated with suspension of *Pto* or *Pma* with OD_{600} = 0.0001. Two days after inoculation, leaf discs were punched out from the inoculated leaves and subjected to bacterial counting by plating bacterial suspension from macerated leaf discs. For each strain:genotype:treatment combination, the bacterial count was measured in at least eight biological replicates in each of at least three independent experiments. The $\log_{10}$-transformed bacterial count (CFU/cm^2) was used in modeling and supplied as raw data (Data S1).

Preprocessing of the sector marker gene expression levels to obtain the sector activity values

The preprocessing of the sector marker gene expression levels were performed in the R environment. First, between-samples normalization based on the normalization gene expression level was performed to make expression level values of the same gene from different samples comparable. The C_t value for each sector marker gene was subtracted from the C_t value for the normalization gene of the same RNA sample to obtain the $\log_2$-transformed expression level value for each marker gene, i.e., $\log_2 ex.l_{sample}^{sector} = C_{t_{sample}}^{norm.gene} - C_{t_{sample}}^{sector}$. Second, each marker gene expression was weakly affected by signals mediated by signaling sectors other than the respective signaling sector (i.e., the marker gene expression levels were very good but not perfect representations of the sector activities). To obtain the expression level value specifically affected by the respective signaling sector, the $\log_2$-transformed expression level value for each genotype carrying the mutant allele for the sector in question was subtracted from the $\log_2$-transformed expression level value for each genotype carrying the wild-type allele for the sector for each treatment:time:replicate combination. For example, to obtain the "mutant-adjusted" $\log_2$-transformed JA marker gene expression level value for *ein2*/*sid2* at 3 hpt with flg22 in

replicate 1 ($m.adj^{JA}_{ein2/sid2,flg22,3hpt,r1}$), the $\log_2$-transformed JA marker gene expression level value for *dde2*/*ein2*/*sid2* at 3 hpt with flg22 in replicate 1 was subtracted from the $\log_2$-transformed JA marker gene expression level value for *ein2*/*sid2* at 3 hpt with flg22 in replicate 1, i.e., $m.adj^{JA}_{ein2/sid2,flg22,3hpt,r1} = \log_2 ex.l^{JA}_{ein2/sid2,flg22,3hpt,r1} - \log_2 ex.l^{JA}_{dde2/ein2/sid2,flg22,3hpt,r1}$. This mutant-adjusting process resulted in expression levels of 0 for the respective sector being assigned to any genotypes containing the mutation corresponding to the respective sector (e.g., *dde2*-containing genotypes for the JA sector marker gene). The 0 values in these genotypes were kept as the fully preprocessed sector activity values for the genotypes, and the mutant-adjusted values in the other genotypes were subjected to further preprocessing. Third, the mutant-adjusted values were used to fit a linear mixed-effects model with the gene:treatment:genotype:time as the fixed effect and the replicate/gene as a random effect. The replicate/gene effect was subtracted from the mutant adjusted value to minimize the replicate effect in the data (the mutant.replicate-adjusted value).

When the standard deviation (SD) values of the mutant.replicate-adjusted values within the same treatment:genotype:time levels were plotted against their means for each marker gene in the MAMP-treated data, the SD values were not homogenous across the mean, except for the ET marker gene (Figure S1B). We decided to monotonically transform the values to obtain the homogenous SD of 1 across the mean for all the marker genes, which justifies use of multiple regression models that include the values from different marker genes. Note that transforming the values to have a homogenous SD is equivalent of making the level of noise constant at any activity level of every signaling sector.

(1) The JA and SA maker gene values tended to have higher SD values for the middle mean values (Figure S1B, first and the fourth panels). We assumed that these marker gene values follow logistic distributions. The first derivative $f'(x) = \frac{ace^{-a(x-b)}}{(1+e^{-a(x-b)})^2}$ of the logistic function $f(x) = \frac{c}{1+e^{-a(x-b)}}$ was fit to the SD vs. mean relationships using the nonlinear regression with least square. The fitted curve *f'(x)* (red curve) and the fitted values of *a*, *b*, and *c* are shown in Figure S1B. The inverse $g^{-1}(x) = \frac{1}{p}\log\left(\frac{x-s}{r-x+s}\right) + q$ of the logistic function $(x) = \frac{r}{1+e^{-p(x-q)}} + s$, where $r = \frac{2}{a}\log\frac{0.95}{0.05}$, $p = \frac{ac}{r}$, $q = \frac{r}{2}$, $s = b - q$ was used for transformation of the mutant.replicate-adjusted values. To moderate the transformation close to the logistic asymptotes, the parts of the inverse function corresponding to the logistic quantiles smaller than bottom 12.5% and larger than the top 12.5% were replaced with linear extensions of the inverse function at the boundaries.

(2) The PAD4 marker gene values tended to have an approximately linear relationship between the SD and mean values (Figure S1B, third panel) although the fitted derivative of the logistic function (red curve) and the associated parameter values as in procedure (1) are shown in the panel. We fitted a linear regression (intercept, *t*; slope *u*) instead, and the shifted log-transformation $h(x) = \frac{1}{u}\log(x + \frac{t}{u})$ was used to transform the mutant.replicate-adjusted values. To moderate the transformation near $x = -\frac{t}{u}$, the part corresponding to $x < x_{max}/4$ were replaced with linear extension of the shifted log-transformation at the boundary.

(3) The ET marker gene values appeared to already have a homogenous SD across the mean (Figure S1B, second panel). Therefore, the mutant.replicate-adjusted values were linearly scaled to make the average SD 1.

After the above transformation procedures, a constant was added to set the minimum value for each marker gene 0 where the minimum value was negative. These fully preprocessed values are referred to as the sector activity values and were used in the modeling process (Data S2). To test the homogeneity of the SD of the sector activity, polynomial regressions of up to the fourth order were fit with the SD as the response and the mean as the explanatory variable, and the model with the lowest AIC was selected for each marker gene (Figure S1C). For each marker gene, the model with only an intercept, of approximately 1, had the lowest AIC (blue line), which indicates the transformed values have approximately homogenous SDs. Figure S1D shows the plots of the values after the transformation vs. the values before.

Multiple regression models

To construct a dynamic signaling network model, a multiple regression model was fit to the activity values of each of four signaling sectors. A multiple regression model was also fit to the bacterial counts of each strain, to construct a unified network capturing both the sector activities and the immunity levels across four treatments and sixteen genotypes. The starting models are depicted in Figure S1E.

We assume that the entire signaling network mediating the phenomena of interest is a web-like network (Sato et al., 2010). The subnetwork composed of the four sectors forms a relative bottleneck (though not absolute bottleneck) in the network, thus, the major part of the network output (i.e., the immunity level) requires the four-sector subnetwork (Tsuda et al.,

2009). Since a complex subnetwork exists between the PRRs and the four-sector subnetwork, some signals initiated by the PRR activation reach the four-sector subnetwork fast and other signals reach the four-sector subnetwork slowly. If the slow signals arrive in the four-sector subnetwork after 3 hpt, a model that lacks the links from the treatments to the 9-hpt nodes would not integrate the slow signal information in processing the network response. This is the reason the links from the treatments to the 9-hpt nodes were included.

Similarly, even among the four sectors, as each sector forms a complex sub-subnetwork, some signals reach other sectors fast and other signals reach them slowly. Fast signals are represented by the links between the sector nodes within a single time point. We assumed that the values from the same time point for other sectors can approximate slightly earlier values for the sectors. Slow signals are represented by the links from the 3-hpt to the 9-hpt sector nodes. Furthermore, there is another complex subnetwork between the four-sector subnetwork and the highly summarized phenotype of induced immunity, and we assumed that both 3-hpt and 9-hpt sector activities could affect the immunity level. Thus, all the links in the full starting models are biologically justified.

Multiple regression models with L1-norm (Lasso) regularization (Friedman et al., 2010) were used to avoid overfitting; models were formulated via

$$\widehat{\boldsymbol{\beta}}^{lasso} = \min_{(\beta_0,\boldsymbol{\beta})\in\mathbb{R}^{p+1}} \left[\frac{1}{2N} \sum_{i=1}^{N} \left(y_i^m - \beta_0 - \boldsymbol{x_i^T \beta} \right)^2 + \lambda \|\boldsymbol{\beta}\|_{l_1} \right]$$

where p is the total number of initial parameters excluding an intercept, N is the total number of cases covering all possible combinatorial conditions, β_0 is an intercept, $\boldsymbol{\beta}$ is the parameter vector to be estimated (i.e., the links in Figure S1E). The explanatory variable $\boldsymbol{x_i}$ consists of either binary indicators for treatment-specific variables or continuous variables corresponding to the

sector activity. y_i^m is the response, which is either an actual activity value for m sector or an actual $\log_{10}$-transformed count of m bacterial strain. λ is the penalty factor balancing the prediction error and the model complexity (Friedman et al., 2010).

Specifically, for each sector, we modeled its 3-hpt activity value as a linear function of the input MAMP signal and the activity values of the other sectors at 3 hpt. Nine hpt activity value of each sector was modeled as a linear function of the input MAMP signal and the 3- and 9-hpt activity values of the other sectors. A complete formulation of the regression model for JA sector (1st panel in Figure S1E) was:

$$y^{JA} = \beta_0^{JA} + 1_{3h} \cdot 1_f \cdot \beta_{f,JA_3} + 1_{3h} \cdot 1_e \cdot \beta_{e,JA_3} + 1_{3h} \cdot 1_c \cdot \beta_{c,JA_3} + 1_{3h} \cdot ET_3 \cdot \beta_{ET_3,JA_3} + 1_{3h} \cdot PAD4_3 \cdot \beta_{PAD4_3,JA_3} + 1_{3h} \cdot SA_3 \cdot \beta_{SA_3,JA_3} + 1_{9h} \cdot 1_m \cdot \beta_{m,JA_9} + 1_{9h} \cdot 1_f \cdot \beta_{f,JA_9} + 1_{9h} \cdot 1_e \cdot \beta_{e,JA_9} + 1_{9h} \cdot 1_c \cdot \beta_{c,JA_9} + 1_{9h} \cdot ET_3 \cdot \beta_{ET_3,JA_9} + 1_{9h} \cdot PAD4_3 \cdot \beta_{PAD4_3,JA_9} + 1_{9h} \cdot SA_3 \cdot \beta_{SA_3,JA_9} + 1_{9h} \cdot ET_9 \cdot \beta_{ET_9,JA_9} + 1_{9h} \cdot PAD4_9 \cdot \beta_{PAD4_9,JA_9} + 1_{9h} \cdot SA_9 \cdot \beta_{SA_9,JA_9}.$$

Where β_0 is an intercept; 1_{3h} and 1_{9h} are binary indicator variables for 3 hpt and 9 hpt respectively; 1_m, 1_f, 1_e, and 1_c are binary indicator variables for mock, flg22, elf18, and chitosan treatment, respectively; ET_3, and ET_9 represent the ET sector activities at 3 hpt and 9 hpt, respectively; $\beta_{s,t}$ is a parameter that corresponds to the signal flow from a source node s to a target node t for the JA sector activity. The models for ET, PAD4, and SA sector (2nd, 3rd, and 4th panels in Figure S1E) were formulated similarly:

$$y^{ET} = \beta_0^{ET} + 1_{3h} \cdot 1_f \cdot \beta_{f,ET_3} + 1_{3h} \cdot 1_e \cdot \beta_{e,ET_3} + 1_{3h} \cdot 1_c \cdot \beta_{c,ET_3} + 1_{3h} \cdot JA_3 \cdot \beta_{JA_3,ET_3} + 1_{3h} \cdot PAD4_3 \cdot \beta_{PAD4_3,ET_3} + 1_{3h} \cdot SA_3 \cdot \beta_{SA_3,ET_3} + 1_{9h} \cdot 1_m \cdot \beta_{m,ET_9} + 1_{9h} \cdot 1_f \cdot \beta_{f,ET_9} + 1_{9h} \cdot 1_e \cdot \beta_{e,ET_9} + 1_{9h} \cdot 1_c \cdot \beta_{c,ET_9} + 1_{9h} \cdot JA_3 \cdot \beta_{JA_3,ET_9} + 1_{9h} \cdot PAD4_3 \cdot \beta_{PAD4_3,ET_9} + 1_{9h} \cdot SA_3 \cdot \beta_{SA_3,ET_9} + 1_{9h} \cdot JA_9 \cdot \beta_{JA_9,ET_9} + 1_{9h} \cdot PAD4_9 \cdot \beta_{PAD4_9,ET_9} + 1_{9h} \cdot SA_9 \cdot \beta_{SA_9,ET_9};$$

$$y^{PAD4} = \beta_0^{PAD4} + 1_{3h} \cdot 1_f \cdot \beta_{f,PAD4_3} + 1_{3h} \cdot 1_e \cdot \beta_{e,PAD4_3} + 1_{3h} \cdot 1_c \cdot \beta_{c,PAD4_3} + 1_{3h} \cdot JA_3 \cdot \beta_{JA_3,PAD4_3} + 1_{3h} \cdot ET_3 \cdot \beta_{ET_3,PAD4_3} + 1_{3h} \cdot SA_3 \cdot \beta_{SA_3,PAD4_3} + 1_{9h} \cdot 1_m \cdot \beta_{m,PAD4_9} + 1_{9h} \cdot 1_f \cdot \beta_{f,PAD4_9} + 1_{9h} \cdot 1_e \cdot \beta_{e,PAD4_9} + 1_{9h} \cdot 1_c \cdot \beta_{c,PAD4_9} + 1_{9h} \cdot JA_3 \cdot \beta_{JA_3,PAD4_9} + 1_{9h} \cdot ET_3 \cdot$$

$\beta_{ET_3,PAD4_9} + 1_{9h} \cdot SA_3 \cdot \beta_{SA_3,PAD4_9} + 1_{9h} \cdot JA_9 \cdot \beta_{JA_9,PAD4_9} + 1_{9h} \cdot ET_9 \cdot \beta_{ET_9,PAD4_9} + 1_{9h} \cdot SA_9 \cdot \beta_{SA_9,PAD4_9}$;

$y^{SA} = \beta_0^{SA} + 1_{3h} \cdot 1_f \cdot \beta_{f,SA_3} + 1_{3h} \cdot 1_e \cdot \beta_{e,SA_3} + 1_{3h} \cdot 1_c \cdot \beta_{c,SA_3} + 1_{3h} \cdot JA_3 \cdot \beta_{JA_3,SA_3} + 1_{3h} \cdot ET_3 \cdot \beta_{ET_3,SA_3} + 1_{3h} \cdot PAD4_3 \cdot \beta_{PAD4_3,SA_3} + 1_{9h} \cdot 1_m \cdot \beta_{m,SA_9} + 1_{9h} \cdot 1_f \cdot \beta_{f,SA_9} + 1_{9h} \cdot 1_e \cdot \beta_{e,SA_9} + 1_{9h} \cdot 1_c \cdot \beta_{c,SA_9} + 1_{9h} \cdot JA_3 \cdot \beta_{JA_3,SA_9} + 1_{9h} \cdot ET_3 \cdot \beta_{ET_3,SA_9} + 1_{9h} \cdot PAD4_3 \cdot \beta_{PAD4_3,SA_9} + 1_{9h} \cdot JA_9 \cdot \beta_{JA_9,SA_9} + 1_{9h} \cdot ET_9 \cdot \beta_{ET_9,SA_9} + 1_{9h} \cdot PAD4_9 \cdot \beta_{PAD4_9,SA_9}$.

Given each of the regression model formulations incorporated with Lasso regularization, we used a bootstrap aggregation approach, called Bagging (Hastie et al., 2009), for measuring test errors with 1000 rounds of bootstrapping and chose an optimal structure (significant parameters) for each sector as follows. Several tens of candidate penalty factors, $\lambda \in (0.001,1.5)$, were first extracted based on an entire set of sector activity values. In each round of bootstrapping for each sector activity model, 32 treatment:genotype combinations (4 treatments x 8 genotypes; the preprocessed dataset does not include 8 genotypes containing the mutation for the modeled sector) were randomly sampled with replacement, and the data corresponding to the sampled treatment:genotype combinations were used as a training dataset, which was used to fit the regression model with each λ value. The sector activity values of the treatment: genotype combinations that were held-out from the training dataset were predicted using the obtained model for each λ value. After this procedure was repeated 1000 times, the median of the predicted values for each treatment:genotype:time combination was selected as a test dataset for each λ value. The same procedure was applied to the other sector activity models, and the test datasets of all the sector activity models were aggregated into the final test dataset for each λ value. Among the models obtained with different λ values, the model with the largest λ that yielded a PCC prediction performance within the 95 % confidence interval of the best measured PCC across all models was selected (Friedman et al., 2010). The selected model structure (a set

of non-zero parameters) was refit to the entire sector activity dataset using ordinary least square (See Table S1A for the mean estimates of the parameters and their confidence intervals). Figure S2D shows the fitted values of the model with these parameter values.

To model immunity levels against each of two bacterial strains, we fit a separate multiple regression model with the model-predicted activity values of the four sectors as the explanatory variables to the $\log_{10}$-transformed bacterial count data. First, all sector activity values were predicted using the process described above, except that zeros were assigned for any sector activities for the genotype containing the mutation for the sector. In each regression model for a bacterial strain, an intercept for the bacterial count in the quadruple mutant with mock treatment was included, and three binary indicators were used to capture MAMP-specific effects in the quadruple mutant that were not be explained by the four sectors. All parameters except for the intercept were multiplied by -1 so that positive values represent positive contributions to plant immunity. The *Pto*-specific starting model (Figure 1B and Figure S1E, fifth panel) was formulated as

$$y^{pto} = \beta_0 - (1_f \cdot \beta_{f,pto} + 1_e \cdot \beta_{e,pto} + 1_c \cdot \beta_{c,pto} + \widehat{JA_3} \cdot \beta_{JA_3,pto} + \widehat{ET_3} \cdot \beta_{ET_3,pto} + \widehat{PAD_3} \cdot \beta_{PAD_3,pto} + \widehat{SA_3} \cdot \beta_{SA_3,pto} + \widehat{JA_9} \cdot \beta_{JA_9,pto} + \widehat{ET_9} \cdot \beta_{ET_9,pto} + \widehat{PAD_9} \cdot \beta_{PAD_9,pto} + \widehat{SA_9} \cdot \beta_{SA_9,pto})$$

Where β_0 is an intercept; 1_f, 1_e, and 1_c are binary indicator variables for flg22, elf18, and chitosan treatment, respectively; $\widehat{JA_3}$, and $\widehat{JA_9}$ represent the predicted activity values of JA sector marker at 3 hpt and 9 hpt, respectively; $\beta_{s,t}$ is a explanatory parameter for the effect from a sector node s to a target node t on the immunity level against *Pto* strain. Similarly, the *Pma*-specific starting model (Figure S1E, sixth panel) was formulated as follows:

$$y^{pma} = \beta_0 - (1_f \cdot \beta_{f,pma} + 1_e \cdot \beta_{e,pma} + 1_c \cdot \beta_{c,pma} + \widehat{JA_3} \cdot \beta_{JA_3,pma} + \widehat{ET_3} \cdot \beta_{ET_3,pma} + \widehat{PAD_3} \cdot \beta_{PAD_3,pma} + \widehat{SA_3} \cdot \beta_{SA_3,pma} + \widehat{JA_9} \cdot \beta_{JA_9,pma} + \widehat{ET_9} \cdot \beta_{ET_9,pma} + \widehat{PAD_9} \cdot \beta_{PAD_9,pma} + \widehat{SA_9} \cdot \beta_{SA_9,pma})$$.

For each strain-specific model, Bagging with 1000 rounds of bootstrapping was applied to find the best model structure and least squares was used to estimate the selected parameters with the complete set of bacterial counts, similarly to the procedure described above for the sector activity models (see Table S1B for the mean estimates for the parameters and their confidence intervals). Figure S2C shows the fitted values of the model with these parameter values.

Evaluation of the prediction accuracy

To assess the predictive power of the network model, we also used a Bagging approach by repeatedly training the model of the selected structure (Figure 2A) with sampled data and evaluating their performance by prediction of the out-of-bag (held-out) data. In each bootstrapping step, the treatment:genotype combinations were randomly sampled with replacement, and the data corresponding to the sampled treatment:genotype combinations were used as a training dataset. The models that were fit to the training dataset were used to predict the held-out data. This process was repeated 1000 times, and the final prediction of the sector activity value for each of 256 sector:treatment:genotype:time combinations (4 sectors x 4 treatments x 8 genotypes x 2 time points) or the bacterial count for each of 128 treatment:genotype:strain combinations (4 treatments x 16 genotypes x 2 strains) was obtained by taking the median over all predicted values for the instance. The final predicted values obtained from the Bagging procedure were then compared with the averages of the

corresponding observed values by calculating a PCC between them (prediction accuracy of the sector activities and the immunity levels in Figures 2B and 2C, respectively).

A signaling network model based on a Bayesian network approach

We also modeled the immune network using a Bayesian network approach. Like the starting structure of the regression model, the structure of the Bayesian network was constrained to have four layers: (1) an input layer with one ternary node for three MAMPs, (2) an activation layer with four binary nodes of the four sectors at 3 hpt, (3) a cross-talk layer with four binary nodes of the four sectors at 9 hpt, and (4) an output layer with two continuous nodes for log-transformed bacterial counts of two bacterial strains (pto and pma). Two components of a Bayesian network model are the network structure, which defines conditional dependence relationships between the variables being modeled, and the conditional probability tables, which quantify these dependencies. We inferred both the structure of the network and the optimal conditional probability tables given the proper structure. For inference of the structure, rather than using a Bayesian structure learning approach (Koller and Friedman, 2009), a regularized linear modeling approach, an Elastic Net, was used (Friedman et al., 2010) to reduce the search space to a small set of structures that reasonably captured relationships between the network sectors. The conditional probability parameters in these candidate structures were fit to the observed data, and the inferred models were assessed by cross-validation. Further details are described below.

Data preprocessing

The mutant-adjusted values of the sector marker gene expression levels (See *Preprocessing of the sector marker gene expression levels to obtain the sector activity values*)

were used as the sector activity values in this section of "A signaling network model based on a Bayesian network approach". The minimum and the maximum values of each signaling sector across 64 different treatment:genotype:time conditions (4 treatments x 8 genotypes x 2 time points) were converted to 0 and 1 of the activation probability, respectively, by linear mapping. For example, $p_{JA_t}^{act} = a \cdot s_{JA_t}^{exp} + b$ where $p_{JA_t}^{act}$ was an activation probabilities of the JA sector at time *t*, where $s_{JA_t}^{exp}$ is an adjusted expression value of the JA sector marker at *t* time, with *a* = 0.173 and *b* = -0.202. The mapping parameter values for the other sectors were: *a* = 0.184, *b* = -0.021 for the ET sector; *a* = 0.174, *b* = 0.031 for the PAD4 sector; *a* = 0.065, *b* = 0.092 for the SA sector. Although the activation probabilities of each sector at 3 hpt considerably varied across the genotypes, we only considered the wild-type activation probability values for the (3-hpt) activation nodes for the sake of the simple structure with directed acyclic graphs (Koller and Friedman, 2009). All activation probabilities of each sector with the genotypes containing the mutation for the sector were set to zero. Only the data from the three MAMP (flg22, elf18, and chitosan) were used for modeling.

For the immunity levels, we chose the same number, 24, of replicates across all treatment:genotype:strain combinations In any conditions with more than 24 replicates, we first filtered replicates based on z-scores, satisfying

$$z_i = \frac{y_i - \mu}{\sigma} \leq 2$$

where μ and σ are a mean and a standard deviation, respectively, of all data for the treatment:genotype:strain combination, and z_i is a z-score of y_i bacterial count. 24 replicates were then randomly chosen from the set that passed the filter.

Elastic Net

To extract a set of candidate Bayesian network structures, we applied an Elastic Net (Friedman et al., 2010). The Elastic Net structure was the same as that described above for the Bayesian network constraints except three MAMP nodes instead of one were used in the input layer:

$V = \{V_{in}, V_{act}, V_{cross}, V_{out}\} = \{v_1, \dots, v_{13}\}$

$V_{in} = \{v_1, v_2, v_3\}$; $V_{act} = \{v_4, v_5, v_6, v_7\}$; $V_{cross} = \{v_8, v_9, v_{10}, v_{11}\}$; and $V_{out} = \{v_{12}, v_{13}\}$.

V_{in}, V_{act}, V_{cross}, and V_{out} correspond to the input, activation, cross-talk, and output layers, respectively. The Elastic Net problem is defined as

$$\min_{(\beta_0, \boldsymbol{\beta}) \in \mathbb{R}^{p+1}} \frac{1}{2N_E} \sum_{i=1}^{N_E} (y_i - \beta_0 - \boldsymbol{x}_i^T \boldsymbol{\beta})^2 + \lambda \left((1-\alpha) \cdot \frac{1}{2} \|\boldsymbol{\beta}\|_{l_2}^2 + \alpha \|\boldsymbol{\beta}\|_{l_1} \right)$$

where N_E is the total number of instances for the Elastic Net, $\boldsymbol{\beta}$ is a $p \times 1$ vector with p parameters, $\boldsymbol{x}_i$ is a $p \times 1$ vector with p variables capturing variant network structures for an i instance of treatment:genotype:time:replicate or treatment:genotype:strain:replicate combinations, y_i is an actual measurement of the i instance (either an activation probability or a bacterial count), λ is an Elastic Net penalty factor, and α is a balancing factor controlling the compromise between ridge regression ($\alpha = 0$) and lasso regression ($\alpha = 1$) (Friedman et al., 2010). More specifically, $\boldsymbol{x}_i$ has 42 variables, representing states of all possible links: $x_{i,j}$ ($j \in \{1, \dots, 12\}$), links between V_{in} and V_{act}; $x_{i,j}$ ($j \in \{13, \dots, 28\}$), links between V_{act} and V_{cross}; $x_{i,j}$ ($j \in \{29, \dots, 36\}$), links between V_{cross} and V_{out}; $x_{i,j}$ ($j \in \{37, \dots, 42\}$), links between V_{in} and V_{out}. If y_i is either an activation probability at 3 hpt or a bacterial count, $\boldsymbol{x}_i$ is a binary vector containing 1 or 0 according to the i treatment:genotype condition. If y_i is an activation probability at 9 hpt, $\boldsymbol{x}_i$ is a continuous vector which contains $1/m$ (m = 4 for wild type; m = 3 for 4 single mutants; m = 2 for 6 double mutants; m = 1 for 4 triple mutants) or 0 for $x_{i,j}$($j \in$

$\{1, \ldots, 12\}$) and 1 or 0 for $x_{i,j} (j \in \{13, \ldots, 42\})$ according to the i treatment:genotype condition. To integrate two different types of data, the sector activation provability and the $\log_{10}$-bacterial counts, which have different ranges, the activation probabilities was rescaled by multiplying by a scaling factor (1.403) before fitting the Elastic Net. Note that for the Elastic Net, the response does not have to be restricted to [0,1]. This factor was derived by maximizing a correlation between original and rescaled values.

To estimate the model parameters, we used a 6-fold cross-validation (6CV) approach according to the treatment:strain combinations in order to minimize the test error. The quadruple mutant immunity level data were always retained in the 6-fold training data, such that the prediction accuracies of the six models only affected by four sectors were calculated. For example, if bacterial counts of the *Pto* strain in 15 genotypes (all except the quadruple mutant) with flg22 treatment were held-out for the test data, the model was fit to the rest: all activation probabilities of the four sectors in all conditions, bacterial counts in 16 genotypes in the other five treatment:strain combinations, and bacterial counts in the quadruple mutant of the flg22:pto combination. With an α ($\forall \alpha \in [0.01, 1]$), we applied a coordinate descent algorithm for finding a set of appropriate λs to be searched ($\forall \lambda \in (0.005, 100)$) based on the entire data (Friedman et al., 2010). Given the two factors, the model was fit to the data for 5 out of 6 treatment:strain combinations (the training data) and tested the predictions of the held-out data. With a selection of λ resulting in the smallest mean square test error from 6CV given α, we refit the Elastic Net to obtain the model structures and the parameters with the penalty factors (Friedman et al., 2010). Among these fitted models with different levels of sparsity, we chose 10 candidate structures ($\boldsymbol{G}_B^m$, $m \in \{1, \ldots, 10\}$) that retained distinct sets of non-zero parameters for the inter-

connectedness between four sectors as an initial set of model structures for the Bayesian network.

Data preparation for the Bayesian network

The Bayesian network model has 11 network components: one ternary node (X_1) for three MAMP treatments as input signals; four binary nodes ($X_i, i \in \{2, \dots, 5\}$) at early states (3 hpt) and four binary nodes ($X_i, i \in \{6, \dots, 9\}$) at late states (9 hpt) describing dynamics of the four sectors; two continuous nodes ($X_i, i \in \{10,11\}$) for two bacterial strains. The Bayesian network model was designed to capture the dependency between input signals (three treatments) and outcomes (immunity levels against two bacterial strains) only through the four sectors. Thus, given a MAMP treatment, the effects that were not explained by the four-sector network (remainder effects) were estimated by taking the differences between two means of bacterial counts with mock and MAMP treatments in the quadruple mutant.

In each treatment:genotype combination, 24 instances, each of which consists of a set of states of each of the 11 components of the network, were generated as follows:

$$\boldsymbol{x} = [x_1, \dots, x_{11}] = [x^t_{MAMP}, x^b_{JA_{3h}}, x^b_{ET_{3h}}, x^b_{PAD4_{3h}}, x^b_{SA_{3h}}, x^b_{JA_{9h}}, x^b_{ET_{9h}}, x^b_{PAD4_{9h}}, x^b_{SA_{9h}}, x^c_{pto}, x^c_{pma}]$$

where x^t_{MAMP} is a ternary variable ($x^t_{MAMP} \in \{1,2,3\}$: 1, flg22; 2, elf18; 3, chitosan), $x^b_{s_t}$ is a binary variable representing an on or off state of *s* sector at time *t* ($x^b_{s_t} \in \{0,1\}$: 0, inactivation state or mutation; 1, activation state), x^c_p is a continuous variable representing the bacterial count of *p* strain ($x^c_p \in \mathbb{R}$). For example, an instance for chitosan:wild-type condition is described as

$$\boldsymbol{x} = [3, 1, 1, 1, 0, 1, 1, 1, 1, 4.08, 4.54].$$

To derive the binary states from the observed continuous data, we first generated the corresponding number of zeros and ones according to the activation probabilities (e.g. If $p^{act}_{s_t} = 0.25$, the $x^b_{s_t}$ variables in 24 instances under the condition consist of 6 ones and 18 zeros). Within

24 instances under each condition, we randomly assigned the zeros and ones into the binary variables ($x_{i,j}, j \in \{2, \dots, 9\}$). In total, we generated a set of instances covering all data 100 times ($\boldsymbol{x}_i, i \in \{1, \dots, 100\}$) to prevent from any bias due to the discretization process.

Parameter inference

A set of n_B random variables ($\boldsymbol{X} = \{X_1, \dots, X_{n_B}\},\ n_B = 11$) is a Bayesian network with respect to a directed acyclic graph ($\boldsymbol{G}_B$) if its joint probability density function can be written as

$$p(\boldsymbol{X}) = \prod_{i=1}^{n_B} p\left(X_i | X_j\right) \text{ for } j \in \{I[pa(X_i)]\}$$

where $pa(X_i)$ is a set of parents of X_i and $I[\,]$ is an index function, satisfying a local Markov property: each variable is conditionally independent of its non-descendants given its parent variables,

$$X_i \perp X_j | X_k \text{ for } j \in \{I[\boldsymbol{X} \backslash de(X_i)]\}\ and\ k \in \{I[pa(X_i)]\}$$

where $de(X_i)$ is a set of descendants of X_i (Koller and Friedman, 2009).

To infer the parameters, conditional probabilities of all variables given a network structure $\boldsymbol{G}_B^m$, a network with random parameters was created first. The parameter sets for nine discrete nodes ($\boldsymbol{\theta}_{i,j}, j = \{1, \dots, 9\}$) were generated based on a likelihood equivalent uniform Bayesian Dirichlet prior (Koller and Friedman, 2009) and the parameter sets for last two continuous nodes ($\boldsymbol{\theta}_{i,j}, j = \{10,11\}$) were generated from normal distributions. We then found the maximum likelihood estimates (MLEs) of the parameters,

$$\tilde{\boldsymbol{\theta}}_{i,j}^m = \max_{\boldsymbol{\theta}_{i,j}} p\left(\boldsymbol{x}_{i,j} | \boldsymbol{G}_B^m, \boldsymbol{\theta}_{i,j}\right) = \max_{\boldsymbol{\theta}_{i,j}} \sum_{k=1}^{N_B} p\left(x_{i,j,k} | \boldsymbol{G}_B^m, \boldsymbol{\theta}_{i,j}\right)$$

where $\boldsymbol{x}_{i,j}$ is a set of instances of j random variable in an i set of instances, $\boldsymbol{\theta}_{i,j}$ is a conditional probability distribution of j random variable ($j \in \{1, \dots, 11\}$) with i set of instances ($i \in$

$\{1, \ldots, 100\}$), $\boldsymbol{G}_B^m$ is a given m structure ($m \in \{1, \ldots, 10\}$), $\widetilde{\boldsymbol{\theta}}_{i,j}^m$ is the estimated $\boldsymbol{\theta}_{i,j}$, maximizing the posterior conditional probability distribution, $p\left(\boldsymbol{x}_{i,j} | \boldsymbol{G}_B^m, \boldsymbol{\theta}_{i,j}\right)$, N_B is the total number of instances and $x_{i,j,k}$ is a k instance in $\boldsymbol{x}_{i,j}$ ($k \in \{1, \ldots, N_B\}$). In our case, the states of all nodes were fully observed, such that the maximum likelihood estimates were counts of the number of instances with the given combination of states. Note that in case of a zero instance due to perturbation, we updated the parameters only for the descendent nodes of the perturbed node (Koller and Friedman, 2009).

Relative conditional dependencies

To explore strengths of conditional effects between two connected nodes, we defined several different types of regulatory effects related to links (visualized in Figure S2A), which could be calculated directly from the learned Bayesian network models:

1. For the links between X_1 and X_i ($i \in \{2, \ldots, 5\}$), the strength of the signaling activation of s_1 sector at 3 hpt under *t* MAMP treatment can be calculated as

$$\widetilde{\omega}_{MAMP, s_{1,3h}} = p\left(x_{s_{1,3h}}^b = 1 | x_{MAMP}^t = t, \boldsymbol{G}_B^m, \widetilde{\boldsymbol{\theta}}_i^m\right),$$

   where $\widetilde{\omega}_{a,d}$ is a measured weight of the link between *a* and *d*.

2. For the links between X_i and X_{i+4} ($i \in \{2, \ldots, 5\}$), the strength of the direct regulation of the $s_1$sector from 3 hpt to 9 hpt can be measured as

$$\widetilde{\omega}_{s_{1,3h}, s_{1,9h}}^i = \log_2 \left(\frac{p\left(x_{s_{1,9h}}^b = 1 \middle| x_{s_{1,3h}}^b = 1,\ x_{s_{i,3h}}^b = 0, \boldsymbol{G}_B^m, \widetilde{\boldsymbol{\theta}}_i^m\right)}{p\left(x_{s_{1,9h}}^b = 0 \middle| x_{s_{1,3h}}^b = 1,\ x_{s_{i,3h}}^b = 0, \boldsymbol{G}_B^m, \widetilde{\boldsymbol{\theta}}_i^m\right)} \right),$$

$$s_{i,3h} \in pa\left(s_{1,9h}\right) \backslash s_{1,3h} \text{ if } \left|pa\left(s_{1,9h}\right)\right| > 1,$$

   where $\widetilde{\omega}_{a,d}^i$ is a measured weight of the link between *a* and *d* based on $\boldsymbol{x}_i$.

3. For the links between X_i ($i \in \{2, \ldots, 5\}$) and X_j ($j \in \{6, \ldots, 9\}$), the strength of the cross-talk regulation of s_1 sector at 9 hpt from s_2 sector at 3 hpt can be measured as

$$\widetilde{\omega}^{i}_{s_{2,3h},s_{1,9h}} = \log_2\left(\frac{p\left(x^b_{s_{1,9h}}=1\middle|x^b_{s_{1,3h}}=1,\ x^b_{s_{2,3h}}=1,\ x^b_{s_{i,3h}}=0,\boldsymbol{G}^m_B,\widetilde{\boldsymbol{\theta}}^m_i\right)}{p\left(x^b_{s_{1,9h}}=0\middle|x^b_{s_{1,3h}}=1,\ x^b_{s_{2,3h}}=1,\ x^b_{s_{i,3h}}=0,\boldsymbol{G}^m_B,\widetilde{\boldsymbol{\theta}}^m_i\right)}\right)$$

$$-\log_2\left(\frac{p\left(x^b_{s_{1,9h}}=1\middle|x^b_{s_{1,3h}}=1,\ x^b_{s_{2,3h}}=0,\ x^b_{s_{i,3h}}=0,\boldsymbol{G}^m_B,\widetilde{\boldsymbol{\theta}}^m_i\right)}{p\left(x^b_{s_{1,9h}}=0\middle|x^b_{s_{1,3h}}=1,\ x^b_{s_{2,3h}}=0,\ x^b_{s_{i,3h}}=0,\boldsymbol{G}^m_B,\widetilde{\boldsymbol{\theta}}^m_i\right)}\right),$$

$$s_{i,3h} \in pa\left(s_{1,9h}\right)\backslash s_{1,3h} \text{ if } \left|pa\left(s_{1,9h}\right)\right| > 1.$$

4. For the links between X_i ($i \in \{6,\dots,9\}$) and X_j ($j \in \{10,11\}$), the strength of the relative contributions of $s_1$sector to the immunity level against bacterial strain p can be measured as

$$\widetilde{\omega}_{s_{1,9h},p} = -\log_2\left(\frac{\widetilde{m}_p \text{ given } x^b_{s_{1,9h}}=1,\ x^b_{s_{i,9h}}=0,\boldsymbol{G}^m_B}{\widetilde{m}_p \text{ given } x^b_{s_{1,9h}}=0,\ x^b_{s_{i,9h}}=0,\boldsymbol{G}^m_B}\right), i \in \{2,3,4\},$$

where $\widetilde{m}_p$ is an estimated mean of X_i ($i \in \{n-1,n\}$) based on the condition.

Model evaluation and selection

We evaluated each Bayesian network model with the estimated parameters ($\widetilde{\boldsymbol{\theta}}^m_i$) given the structure ($\boldsymbol{G}^m_B$) in five different ways:

1. calculating a log-likelihood (ll_i),
2. using Bayesian information criteria (BIC_i),
3. calculating two Spearman's rank correlation coefficients to measure both a training set accuracy, r_s(3CV, trng, activation probabilities), and a test set accuracy, r_s(3CV, test, activation probabilities), of predicting activation probabilities of the four sectors with 3CV across the three MAMP treatments,
4. calculating two Spearman's rank correlation coefficients to measure both a training set accuracy, r_s(6CV, trng, immunity levels), and a test set accuracy, r_s(6CV, test, immunity levels), of predicting log-transformed bacterial counts of two strains with 6CV across the six MAMP:strain combinations, and

5. computing the statistical significance of conditional dependencies for links between any two sector nodes.

Each of the evaluation methods is described in detail below.

The log-likelihood with $\boldsymbol{x}_i$ instances was defined as

$$ll_i = \log \prod_{k=1}^{N_B} p\left(\boldsymbol{x}_{i,k} | \boldsymbol{G}_B^m, \widetilde{\boldsymbol{\theta}}_i\right) = \sum_{j=1}^{n} \sum_{k=1}^{N_B} \log p\left(x_{i,j,k} | \boldsymbol{x}_{i,pa(j),k}, \widetilde{\boldsymbol{\theta}}_{i,j}\right)$$

where $\boldsymbol{x}_{i,pa(j),k}$ is a set of instances of all the parent nodes of j random variable in an i set of instances.

Given the log-likelihood with $\boldsymbol{x}_i$ instances, the BIC_i was calculated as

$$BIC_i = \frac{1}{N_B} \sum_{k=1}^{N_B} \log p\left(\boldsymbol{x}_{i,k} | \boldsymbol{G}_B^m, \widetilde{\boldsymbol{\theta}}_i\right) - \frac{n_p^m}{2} \log N_B$$

where n_p^m is the total number of estimated parameters given the structure $\boldsymbol{G}_B^m$.

To explore the prediction accuracy of the activation probabilities of the four sectors with each Bayesian network model given $\boldsymbol{G}_B^m$ and $\boldsymbol{x}_i$, 3 CV was used by splitting entire instances into three parts based on the MAMP treatments,

$$\boldsymbol{x}_i = [\boldsymbol{x}_{i,flg22}, \boldsymbol{x}_{i,elf18}, \boldsymbol{x}_{i,chitosan}]^T.$$

For the k part (held-out test data, $k \in \{1,2,3\}$), we created a network with random parameters (See *Parameter Inference*), estimated the model parameters with the other parts of the instances (training data) by MLEs, and predicted both the training and test data. Two Spearman's rank correlations for the training error and the test error were then calculated between observed and predicted instances. For the prediction accuracy of the log-transformed bacterial counts against two bacterial strains, the same procedures as above were executed to calculate two Spearman's rank correlations with 6CV in terms of treatment:strain combinations,

$$\boldsymbol{x}_i = [\boldsymbol{x}_{i,flg22:pto}, \boldsymbol{x}_{i,elf18:pto}, \boldsymbol{x}_{i,chitosan:pto}, \boldsymbol{x}_{i,flg22:pma}, \boldsymbol{x}_{i,elf18:pma}, \boldsymbol{x}_{i,chitosan:pma}]^T.$$

Note that we selected median values as final values of the four metrics explained above.

Wilcoxon signed rank test was applied to measure the statistical significance of the conditional dependencies among sectors (Siegel, 1956). Specifically, with 100 different measured weights ($\widetilde{\boldsymbol{\omega}}_{a,b}$) of the cross-talk regulation between *a* and *b* in 100 different models based on $\boldsymbol{x}_i$($i \in \{1, \dots, 100\}$), a two-sided rank test was performed of the hypothesis that the values in the vector come from a distribution whose median is zero. To do so, a test statistic *W,* denoted as

$$W = \left| \sum_{i=1}^{n_{rp}} \left[sgn\left(\widetilde{\omega}_{2,i} - \widetilde{\omega}_{1,i}\right) \cdot R_i \right] \right|$$

where n_{rp} is the number of pairs, *sgn* is a sign function, $\widetilde{\omega}_{1,i}$ and $\widetilde{\omega}_{2,i}$ are any paired measurements of the weights, and R_i is the rank of *i* pair, was calculated to obtain a *p*-value. If $p < 10^{-4}$, we designated that the conditional dependence between *a* node and *b* node was significant with the sign. Starting with 10 structures ($\boldsymbol{G}_B^m,\ m \in \{1, \dots, 10\}$) from the Elastic Net, the parameters and the structures of each of the models were evaluated in the five validation criteria. Note that selected Bayesian network models with high prediction accuracy and reasonable complexity (high ll, high r_s (CV, trng) and r_s (CV, test) for both activation probabilities of four sectors and bacterial counts against two strains, and high *BIC*) shared most of significant links for cross-talks among four sectors but also had distinct links, some of which might be insignificant. Thus, extra sets of candidate structures were iteratively extracted by the model consensus, and the models with the structures were evaluated, until the sparsest model having all significant links with high prediction accuracy was selected. The final Bayesian network model selected by the iterative approach is shown in Figure S2A. The same color codes

for nodes and links as in Figure 2A were used. The width and color intensity of each link is proportional to the strength of the conditional association. All labeled values in the links are medians among 100 values from the models with $\boldsymbol{x}_i, i \in \{1, \ldots, 100\}$. The sizes of the sector nodes at both 3 hpt and 9 hpt are proportional to their marginal activation probabilities, $\tilde{p}_{s_t}^{act} = p(s_t = 1)$.

Multiple regression models with the same starting structure as the Bayesian network (Bm-like regression model)

We also implemented multiple regression models starting from the same network structure as the Bayesian network (Fig S2B). Basically, the structure of starting models consists of links connecting between nodes belonging to two neighboring layers. It also contains the direct link from the 3-hpt to the 9-hpt nodes within each sector. Similar to the Bayesian network, only wild-type datasets for the activity levels of the four sectors at 3 hpt were used for capturing relative activation strengths from three different MAMPs. The complete formulations of the sector-specific regression models for JA, ET, PAD4, and SA sector are:

$$y^{JA} = \beta_0^{JA} + 1_{3h} \cdot 1_f \cdot \beta_{f,JA_3} + 1_{3h} \cdot 1_e \cdot \beta_{e,JA_3} + 1_{3h} \cdot 1_c \cdot \beta_{c,JA_3} + 1_{9h} \cdot JA_3 \cdot \beta_{JA_3,JA_9} + 1_{9h} \cdot ET_3 \cdot \beta_{ET_3,JA_9} + 1_{9h} \cdot PAD4_3 \cdot \beta_{PAD4_3,JA_9} + 1_{9h} \cdot SA_3 \cdot \beta_{SA_3,JA_9};$$

$$y^{ET} = \beta_0^{ET} + 1_{3h} \cdot 1_f \cdot \beta_{f,ET_3} + 1_{3h} \cdot 1_e \cdot \beta_{e,ET_3} + 1_{3h} \cdot 1_c \cdot \beta_{c,ET_3} + 1_{9h} \cdot JA_3 \cdot \beta_{JA_3,ET_9} + 1_{9h} \cdot ET_3 \cdot \beta_{ET_3,ET_9} + 1_{9h} \cdot PAD4_3 \cdot \beta_{PAD4_3,ET_9} + 1_{9h} \cdot SA_3 \cdot \beta_{SA_3,ET_9};$$

$$y^{PAD4} = \beta_0^{PAD4} + 1_{3h} \cdot 1_f \cdot \beta_{f,PAD4_3} + 1_{3h} \cdot 1_e \cdot \beta_{e,PAD4_3} + 1_{3h} \cdot 1_c \cdot \beta_{c,PAD4_3} + 1_{9h} \cdot JA_3 \cdot \beta_{JA_3,PAD4_9} + 1_{9h} \cdot ET_3 \cdot \beta_{ET_3,PAD4_9} + 1_{9h} \cdot PAD4_3 \cdot \beta_{PAD4_3,PAD4_9} + 1_{9h} \cdot SA_3 \cdot \beta_{SA_3,PAD4_9};$$

$$y^{SA} = \beta_0^{SA} + 1_{3h} \cdot 1_f \cdot \beta_{f,SA_3} + 1_{3h} \cdot 1_e \cdot \beta_{e,SA_3} + 1_{3h} \cdot 1_c \cdot \beta_{c,SA_3} + 1_{9h} \cdot JA_3 \cdot \beta_{JA_3,SA_9} + 1_{9h} \cdot ET_3 \cdot \beta_{ET_3,SA_9} + 1_{9h} \cdot PAD4_3 \cdot \beta_{PAD4_3,SA_9} + 1_{9h} \cdot SA_3 \cdot \beta_{SA_3,SA_9}.$$

Similarly, the strain-specific regression models for *Pto* and *Pma* are formulated as

$$y^{pto} = \beta_0 - (1_f \cdot \beta_{f,pto} + 1_e \cdot \beta_{e,pto} + 1_c \cdot \beta_{c,pto} + \widehat{JA}_9 \cdot \beta_{JA_9,pto} + \widehat{ET}_9 \cdot \beta_{ET_9,pto} + \widehat{PAD4}_9 \cdot \beta_{PAD4_9,pto} + \widehat{SA}_9 \cdot \beta_{SA_9,pto});$$

$$y^{pma} = \beta_0 - (1_f \cdot \beta_{f,pma} + 1_e \cdot \beta_{e,pma} + 1_c \cdot \beta_{c,pma} + \widehat{JA}_9 \cdot \beta_{JA_9,pma} + \widehat{ET}_9 \cdot \beta_{ET_9,pma} + \widehat{PAD4}_9 \cdot \beta_{PAD4_9,pma} + \widehat{SA}_9 \cdot \beta_{SA_9,pma}) .$$

Given the starting model structures, we applied same modeling procedures and evaluation strategies as the original full regression model (Figure 2A).

Confirmation of model-predicted signaling interactions

SA and JA measurements and analysis

Plants of 16 combinatorial mutants and an *fls2* mutant were used. Three well-expanded leaves per plant were infiltrated with 1 μM flg22, and the infiltrated leaves were harvested at 9 hpt and flash frozen. At the time of flg22 treatment, leaves of untreated plants were harvested for 0 hpt samples. Leaves from four plants of a same genotype were pooled for one biological sample. Three biological replicates were made from independent experiments. The frozen tissue was macerated to powder and freeze-dried. Extraction and determination of SA and JA from Arabidopsis were performed with an UPLC-MS/MS (AQITY UPLC™ System/Quattro Premier XE; Waters) with an ODS column (AQUITY UPLC BEH C18, 1.7 μm, 2.1 × 100 mm, Waters) (Kojima and Sakakibara, 2012). The detailed conditions of UPLC-MS/MS are described previously (Kojima et al., 2009).

A mixed-effects linear model with the genotype:time interaction as the fixed effect and the experiments as a random effect was fit to the SA level values that were $\log_2$-transformed for

data normalization. The mean estimates of the difference between 0 and 9 hpt were derived from this model and used in Figure 3A. The same type of the model was fit to the same dataset except that the *sid2*-containing genotypes were aggregated to one genotype. This second model was used to derive the mean estimates and their standard errors to compare the difference between the genotypes in the difference between 0 and 9 hpt (difference of difference) by two-tailed *t*-test.

For the JA level, only 9-hpt data were used as many 0-hpt JA levels were below detection. Many JA level values from the genotypes containing *dde2* at 9 hpt were also below detection, and all these genotypes were aggregated into one genotype for this reason. Thus, it is very likely that the mean estimate for the aggregated *dde2*-containing genotype is overestimated. A mixed-effect linear model with the genotype as the fixed effect and the experiments as a random effect was fit to the JA level values that were $\log_2$-transformed for data normalization. The mean estimates shown in Figure 3B and the mean estimates and their standard errors of the difference between the genotypes were derived from the model. The latter were used to compare the difference between the genotypes by two-tailed *t*-test.

Differential fragilities of the sectors

We defined differential fragility as the impact of removal of the signaling sector in question on the fragility, which is the phenotypic difference between the presence and absence of the secondary signaling sector. For example, when the ET sector is the sector in question and *i* sector is the secondary sector, the fragilities in the *EIN2* and *ein2* genotypes are calculated as:

Fragility of *EIN2* regarding *i* sector and *t* treatment (*x*-axis in Figure S4B),

$x_{i,t}^{ET} = \left| m_{gene_i,t}^{s} - m_{wildtype,t}^{s} \right|$,

Fragility of *ein2* regarding *i* sector and *t* treatment (*y*-axis in Figure S4B),

$y_{i,t}^{ET} = \left| m_{gene_i/ein2,t}^{s} - m_{ein2,t}^{s} \right|$,

Differential fragility of the ET sector regarding *i* sector and *t* treatment, $y_{i,t}^{ET} - x_{i,t}^{ET}$

where $m_{gene_i,t}^{s}$ is a mean of observed bacterial count of *s* strain (either *Pto* or *Pma*) with the *i* secondary sector removal (*dde2*, *pad4*, or *sid2* for $gene_i$) and treatment *t*. The fragilities were calculated for the JA, PAD4, and SA sectors similarly: $x_{i,j}^{JA} = \left| m_{gene_i,t}^{s} - m_{wildtype,t}^{s} \right|$ and $y_{i,j}^{JA} = \left| m_{gene_i/dde2,t}^{s} - m_{dde2,t}^{s} \right|$ where $gene_i \in \{ein2, pad4, sid2\}$; $x_{i,j}^{PAD4} = \left| m_{gene_i,t}^{s} - m_{wildtype,t}^{s} \right|$ and $y_{i,j}^{PAD4} = \left| m_{gene_i/pad4,t}^{s} - m_{pad4,t}^{s} \right|$ where $gene_i \in \{dde2, ein2, sid2\}$; $x_{i,j}^{SA} = \left| m_{gene_i,t}^{s} - m_{wildtype,t}^{s} \right|$ and $y_{i,j}^{SA} = \left| m_{gene_i/sid2,t}^{s} - m_{sid2,t}^{s} \right|$ where $gene_i \in \{dde2, ein2, pad4\}$. These fragility values were compared between the presence and absence of the sector in question in Figure S4. The mean and standard error of the differential fragility of each sector across the treatments, the strains, and the secondary sectors were calculated separately for the observed data and the model predictions and are shown in Figure 4.

Network activity map

To systematically examine the mechanistic behavior of the network triggered by MAMP inputs, we generated network activity maps to quantitatively visualize the variation in activity levels of components and signal flows among them in specific genotypes after specific treatments. First, predictions of node activities for all 60 conditions (4 treatments x 15 combinatorial genotypes, excluding the quadruple mutant) were made. The signal flow value for each link was calculated by multiplying its estimated parameter value (Table S1) by the predicted activity of the source node. For the two immunity nodes, the constants

($\beta_{f,pto}, \beta_{e,pto}, \beta_{c,pto}, \beta_{f,pma}, \beta_{e,pto}, \beta_{c,pto}$ in Multiple regression models) associated directly with each treatment were subtracted such that our activity maps show the contributions to immunity only explained by the four sectors. For the final network activity maps shown in Figures 5 and S5, the mock treatment map values for the nodes and the links were subtracted from the corresponding MAMP treatment map values of the same genotypes, and the differential values are shown for flg22, elf18, and chitosan treatments in each genotype. Note that in these differential network activity maps, node and link values could be negative. The sizes of the nodes, with the exception of MAMP nodes, were made proportional to their predicted node activity level (either predicted sector activity values or immunity level values). The color intensity and the width of the links in activity maps are proportional to the signal flow value. For a better visualization in the figures, the node sizes are scaled differently between the signaling sector nodes and the immunity nodes, and the color intensities and the widths of the links are scaled differently between the links targeting the signaling sector nodes and those targeting the immunity nodes.

Network model with noise-added data

The standard deviation of the observed data was defined as the standard deviation of the residuals when a linear model with the sector:genotype:treatment:time combinations as the fixed effect was fit to the sector activity data or when a linear model with the genotype:treatment:strain interactions as the fixed effect was fit to the immunity level data. In each different level of artificial noise, we generated 100 different sets of Gaussian noise having a zero mean and a standard deviation k times that of the observed data ($k = 2^{-1}, 2^0, 2^1, 2^2, 2^3$) and added the noise to the observed data. The noise for the sector activity data and the immunity level data were

generated separately since they had different standard deviations. With each set of the 100 different noise-added datasets, the same modeling approach described in Multiple regression models was applied. The structural stability of the original model (Figure 2A) was evaluated by the cosine similarity (uncentered PCC) of the parameter estimates between each of the 100 models and the original model obtained with the data without additional noise (Figure S3A). In one case (k = 2), the distributions of the parameter estimates across the 100 models were compared with the parameter estimates in the original model (Figure S3B).

Treatment-specific network models

We built separate models for different individual MAMP treatments (treatment-specific models) to compare them with the invariant model (the original model, which has the invariant links from the signaling sectors across four treatments). To build each of treatment-specific models, the data specific to one MAMP treatment and the mock data were used to train the multiple regression models similarly to the approach used for the original model (Figure S3C). The sector activities and immunity levels were predicted with each of treatment-specific models in a similar way to one for the original model, and the predictions were compared with the observed means with the same treatment by PCC. For the invariant model, PCCs were calculated between the predictions and the observed means for particular MAMP treatments, separately (Table S3).

A network model without inter-sector links

To show an importance of the cross-talk information among four sectors to improve the prediction accuracy, we first reformulated the multiple regression starting model structure by

removing all the parameters for the links connecting two signaling sector nodes. Given this as the starting model structures, the multiple regression modeling approach similar to that for the original model was applied. The PCCs between observed data and predicted data for the sector activities and immunity levels were calculated (Table S2).

Predicting the sector activities and the immunity levels of a held-out treatment

If the parameter values for the links from the sectors (sector-specific parameter values) are invariant across the treatments, the sector-specific parameter values that are estimated with some MAMP treatments should be able to be used to predict the sector activities and the immunity levels after treatment with a new MAMP across the genotypes, given the parameter values for the links from the new MAMP treatment (new MAMP-specific parameter values). This notion of predictability of the sector activities and the immunity levels with new MAMP treatment was tested by: holding out the data from one of the MAMP treatments in the network modeling for estimation of the sector-specific parameter values; estimating the MAMP-specific parameter values for the held-out MAMP using the wild-type and quadruple mutant data with the held-out MAMP treatment; and predicting the sector activity and immunity level values in the rest of the genotypes with the held-out MAMP treatment.

First, the data from one of the three MAMP treatments were held out from the full dataset (i.e., the resulting dataset contains the data from two MAMP treatments and mock treatment), and the multiple regression models were fit to the dataset with one MAMP treatment held-out, using the approach similar to that used for the original model. The first step yielded the estimates for the sector-specific parameters. Second, multiple regression models in which the values for the sector-specific parameters were fixed to the estimates obtained in the first step were fit using

least square to the sector activity data of the wild-type genotype and the immunity level data of the wild-type and quadruple mutant genotypes with the held-out MAMP treatment. Only the parameter estimates with $p < 0.05$ were considered, and the others were set to 0. The second step yielded the estimates for the new MAMP-specific parameters.

Third, with the parameter values from the first and second steps, the following simultaneous linear equations for the sector activities, $\widehat{\boldsymbol{x}}$, were solved to obtain the predictions of the sector activity values.

$$\boldsymbol{A}\widehat{\boldsymbol{x}} = \boldsymbol{b}$$

where

$$\widehat{\boldsymbol{x}} = \left[\widehat{JA_3}, \widehat{ET_3}, \widehat{PAD4_3}, \widehat{SA_3}, \widehat{JA_9}, \widehat{ET_9}, \widehat{PAD4_9}, \widehat{SA_9}\right]^T,$$

$$\boldsymbol{A} = \begin{bmatrix} -1 & \beta_{ET_3,JA_3} & \beta_{PAD4_3,JA_3} & \beta_{SA_3,JA_3} & 0 & 0 & 0 & 0 \\ \beta_{JA_3,ET_3} & -1 & \beta_{PAD4_3,ET_3} & \beta_{SA_3,ET_3} & 0 & 0 & 0 & 0 \\ \beta_{JA_3,PAD4_3} & \beta_{ET_3,PAD4_3} & -1 & \beta_{SA_3,PAD4_3} & 0 & 0 & 0 & 0 \\ \beta_{JA_3,SA_3} & \beta_{ET_3,SA_3} & \beta_{PAD4_3,SA_3} & -1 & 0 & 0 & 0 & 0 \\ 0 & \beta_{ET_3,JA_9} & \beta_{PAD4_3,JA_9} & \beta_{SA_3,JA_9} & -1 & \beta_{ET_9,JA_9} & \beta_{PAD4_9,JA_9} & \beta_{SA_9,JA_9} \\ \beta_{JA_3,ET_9} & 0 & \beta_{PAD4_3,ET_9} & \beta_{SA_3,ET_9} & \beta_{JA_9,ET_9} & -1 & \beta_{PAD4_9,ET_9} & \beta_{SA_9,ET_9} \\ \beta_{JA_3,PAD4_9} & \beta_{ET_3,PAD4_9} & 0 & \beta_{SA_3,PAD4_9} & \beta_{JA_9,PAD4_9} & \beta_{ET_9,PAD4_9} & -1 & \beta_{SA_9,PAD4_9} \\ \beta_{JA_3,SA_9} & \beta_{ET_3,SA_9} & \beta_{PAD4_3,SA_9} & 0 & \beta_{JA_9,SA_9} & \beta_{ET_9,SA_9} & \beta_{PAD4_9,SA_9} & -1 \end{bmatrix},$$

$$\boldsymbol{b} = [-\beta_0^{JA} - \beta_{MAMP,JA_3},\ -\beta_0^{ET} - \beta_{MAMP,ET_3},\ -\beta_0^{PAD4} - \beta_{MAMP,PAD4_3},\ -\beta_0^{SA} - \beta_{MAMP,SA_3},$$
$$-\beta_0^{JA} - \beta_{m,JA_9} - \beta_{MAMP,JA_9},\ -\beta_0^{ET} - \beta_{m,ET_9} - \beta_{MAMP,ET_9},\ -\beta_0^{PAD4} - \beta_{m,PAD4_9}$$
$$-\beta_{MAMP,PAD4_9},\ -\beta_0^{SA} - \beta_{m,SA_9} - \beta_{MAMP,SA_9}]^T.$$

After solving the equations, all obtained, predicted sector activities were adjusted by adding the difference between maximum values of observed and predicted activities of the sector in that the values of sector activities should be positive. To predict the log-transformed bacterial counts, we calculated the following linear combinations to obtain the predicted immunity level values:

$$\widehat{\boldsymbol{y}} = \begin{bmatrix} \hat{y}^{pto} \\ \hat{y}^{pma} \end{bmatrix} = \begin{bmatrix} \boldsymbol{\beta}^{pto} \\ \boldsymbol{\beta}^{pma} \end{bmatrix} \cdot \begin{bmatrix} 1 \\ 1 \\ \widehat{\boldsymbol{x}} \end{bmatrix}$$

where

$$\boldsymbol{\beta}^{pto} = [\beta_0^{pto},\ \beta_{MAMP,pto}, \beta_{JA_3,pto},\ \beta_{ET_3,pto}, \beta_{PAD4_3,pto}, \beta_{SA_3,pto},$$
$$\beta_{JA_9,pto},\ \beta_{ET_9,pto}, \beta_{PAD4_9,pto}, \beta_{SA_9,pto}],$$
$$\boldsymbol{\beta}^{pma} = [\beta_0^{pma},\ \beta_{MAMP,pma}, \beta_{JA_3,pma},\ \beta_{ET_3,pma}, \beta_{PAD4_3,pma}, \beta_{SA_3,pma},$$
$$\beta_{JA_9,pma},\ \beta_{ET_9,pma}, \beta_{PAD4_9,pma}, \beta_{SA_9,pma}],$$

and $\hat{\boldsymbol{x}}$ is a column vector with the adjusted, predicted values of the sector activities from the above. PCCs were calculated between the observed and predicted values of the sector activities and of the bacterial counts separately for each of three MAMP-held out cases (flg22, elf18, or chitosan held-out) (Figure S3D).

Models based on the data with the limited orders of network perturbation

The benefit of higher orders of network perturbation at the signaling sectors was evaluated by comparing the models fit by the approach similar to the original modeling approach to datasets with limited orders of perturbation (genotype-constrained models; Figures S6A-S6C): (i) the "single-double" dataset consisting of the data for single mutant, and double mutant genotypes, (ii) the "up-to-single" dataset consisting of the data for wild-type and single mutant genotypes, (iii) the "up-to-double" dataset consisting of the data for wild-type, single mutant, and double mutant genotypes, and (iv) the full dataset (up to triple) for comparisons (the original model, Figure 2A). Note that the sector activity data corresponding to each case were extracted from the fully preprocessed sector activity dataset, so that the values were already mutant-adjusted although the data of genotypes for orders of perturbation higher than the specified in the case were needed in this mutant-adjusting step. This is the reason the original model is designated as using up to triple mutants. The genotypes used in particular genotype-constrained cases and provide non-zero values to particular sectors are shown in the table below.

Order	Genotype	Sectors			
		JA	ET	PAD4	SA
wild-type		(ii, iii, iv)	(ii, iii, iv)	(ii, iii, iv)	(ii, iii, iv)
single	*dde2*	0	(i, ii, iii, iv)	(i, ii, iii, iv)	(i, ii, iii, iv)
	ein2	(i, ii, iii, iv)	0	(i, ii, iii, iv)	(i, ii, iii, iv)
	pad4	(i, ii, iii, iv)	(i, ii, iii, iv)	0	(i, ii, iii, iv)
	sid2	(i, ii, iii, iv)	(i, ii, iii, iv)	(i, ii, iii, iv)	0
double	*dde2/ein2*	0	0	(i, iii, iv)	(i, iii, iv)
	dde2/pad4	0	(i, iii, iv)	0	(i, iii, iv)
	dde2/sid2	0	(i, iii, iv)	(i, iii, iv)	0
	ein2/pad4	(i, iii, iv)	0	0	(i, iii, iv)
	ein2/sid2	(i, iii, iv)	0	(i, iii, iv)	0
	pad4/sid2	(i, iii, iv)	(i, iii, iv)	0	0
triple	*dde2/ein2/pad4*	0	0	0	(iv)
	dde2/ein2/sid2	0	0	(iv)	0
	dde2/pad4/sid2	0	(iv)	0	0
	ein2/pad4/sid2	(iv)	0	0	0

The only difference in modeling in the genotype-constrained cases from the original modeling approach is that the largest λ that resulted in the same number of non-zero parameters as that of the original model was used in Lasso regression instead of searching λ values based on test errors. Note that although the total number of the non-zero parameters is the same, the partition between the sector-specific and treatment-specific non-zero parameters could be different (shown in Figure S6A in parentheses). To assess the prediction accuracies of the

genotype-constrained models, a Bagging approach was applied by repeatedly training regression models of the determined structures with sampled data from the corresponding genotype-constrained data, and the model performance was evaluated on the held-out data (prediction accuracies for the sector activity values and the immunity levels in Figure 6A and Figure S6B, respectively, three left cells of the first row for (ii)-(iv)). Since the number of elements in the PCC calculation varies to a great extent, the significance of the PCC ($-\log_{10}P$) instead of the direct PCC value was used in the comparisons.

The Jaccard index was used to compare the structures of two models, *m* and *n*:

$$J_{m,n}(\boldsymbol{\beta}_m^p, \boldsymbol{\beta}_n^p) = \frac{|\boldsymbol{\beta}_m^p \cap \boldsymbol{\beta}_n^p|}{|\boldsymbol{\beta}_m^p \cup \boldsymbol{\beta}_n^p|}$$

where $p \in \{\text{treatment-specific } or \text{ sector-specific}\}$, and $\boldsymbol{\beta}_{m(n)}^p$ is a binary column vector indicating 0 or non-zero for *p* parameters in *m(n)* model. Figure S6A shows that the model structures regarding both the sector-specific and treatment-specific parameters are substantially different in the "(ii) up to single" model from the original model (iv).

When the sector activity values that correspond to the training datasets were predicted, the prediction accuracies between the model with the original model structure and the genotype-constrained model were very similar when each was fit to the genotype-constrained datasets (Figure 6C, left panel). However, when the genotype-constrained models were used to predict the sector activities of the triple mutant genotypes, which were not included in the genotype-constrained datasets (i)-(iii), the "(ii) up to single" model had clearly lower prediction accuracy compared with when the model with the original model structure was trained with the same genotype-constrained dataset (Figure 6C, right panel). The results of similar analysis for the immunity level are shown in Figure S6C.

Effects of multiple modeling factors.

We generalized the analysis of the genotype-constrained models to investigate the impacts of three modeling factors (the order of network perturbation, the number of sectors in the model, and the number of MAMP treatments) on both prediction accuracies and structural similarities. The approach to explore the order of network perturbation is the same as the above genotype-constrained models. To explore the effect of the number of sectors in the model, the starting models in which particular sector(s) and all links connecting to the sectors were removed and the datasets with the data from the genotypes corresponding to the removed sector(s) were used. For example, when a starting mode lacking the PAD4 sector was used, all data from the *pad4*-containing genotypes were removed. To explore the effect of the number of MAMP treatments, the starting models in which particular MAMP treatment(s) and the links from the treatment(s) were removed and the datasets that have the data with the MAMP treatment(s) removed were used. The combination of the order of network perturbation and the number of MAMP treatments and the combination of the number of sectors and the number of MAMP treatments were also explored. In each case, the largest penalty factor λ that resulted in the same number of non-zero parameters as that of the corresponding part of the original model was used in Lasso regression.

Figures S6D and S6E show the significance of the PCC ($-\log_{10}P$) in the evaluation of prediction accuracy for sector activities and immunity levels, respectively. The significance of the PCC instead of the PCC value itself was used because the number of elements in PCC calculation varies to a large extent. Figure S6F shows the Jaccard index compared to the original model with the full dataset for the sector- and treatment-specific parameters separately. In the heatmap figures, a darker color corresponds to a higher value. Figures S6D and S6E also contain

the heatmaps for the prediction of the triple mutant values in the combination of the order of network perturbation and the number of MAMP treatments.

LEGENDS TO SUPPLEMENTARY FIGURES

Figure S1. Modeling approach, related to Figure 1. (A) The sector marker gene expression levels. Each plot shows the expression levels, after between-samples normalization before mutant-adjustment, of the indicated sector marker gene. The wild-type alleles in the genotype are shown by black dots. Each bar represents an observation: black, genotype containing the wild-type allele for the sector; gray, genotype containing the mutant allele for the sector. See key at top for the color-codes for the treatment and the time. (B)-(D) Non-linear transformation of the mutant:replicate-adjusted sector marker gene expression levels. (B) The standard deviation vs. the mean of every treatment:genotype:time combination in each indicated sector before the transformation. The derivative of the logistic function, $f'(x) = \frac{ace^{-a(x-b)}}{(1+e^{-a(x-b)})^2}$, was fit (red curve), and the parameter values, *a*, *b*, and *c*, are shown, except for the ET sector. For the ET sector, a line parallel to the *x*-axis was fit, and its intercept is shown. (C) The standard deviation vs. the mean after the transformation. The blue line shows the best model determined by AIC among those up to the fourth-order polynomial: the best model was a line parallel to the *x*-axis with the intercept ~ 1 for every sector. (D) The transformation function is shown as the values after vs. the values before the transformation for each sector. (E) The starting multiple regression model structures for each target sector or target strain. (F) The final model structure for each target sector or target strain.

Figure S2. Obtained models and the fitted values for the full multiple regression model, related to Figure 2. (A) The model structure obtained by a Bayesian network approach. Red and green directed links represent activation and inhibition. How the link parameter values and the node sizes were calculated are described in "A signaling network model based on a Bayesian network approach". The width and the color intensity of a link are proportional to the link parameter value. (B) The model structure obtained by a regression model approach with the same starting model structure as the Bayesian network model (A) (Bayesian model (Bm)-like regression model). Directional links in red and green represent the significant parameters, indicating activation and inhibition, respectively. The width and color intensity of the links represent parameter values. The links to the immunity nodes are scaled differently from those to the sector nodes for better visualization. The links from the MAMP nodes to the immunity nodes are not shown as they represent the immunity level that is not explained by the four sectors. The estimated mean parameter value for each link is indicated. Note that the predictive power of this model for the sector activities shown as a Pearson correlation coefficient, r_{exp}, = 0.778, is substantially lower than that of the full regression model, which is 0.881. (C) The fitted values of the final multiple regression models for the immunity levels for the genotype:treatment:strain combinations. The wild-type alleles in the genotype are shown by black dots. The treatment is color-coded as shown at the top. Each plot corresponds to the immunity level against each indicated strain. Gray bar, observed immunity level; blue dot, mean of the observations; brown dot, mean estimate and its 95% confidence interval according to the final model. (D) The fitted values of the final multiple regression models for the sector activities for the genotype:treatment:time:sector combinations. The wild-type alleles in the genotype are shown by black dots. The treatment and the time are color-coded as shown at the top. Each plot

corresponds to each indicated sector. Gray bar, observed sector activity value; blue dot, mean of the observations; brown dot, mean estimate and its 95% confidence interval according to the final model.

Figure S3. Analysis of the full multiple regression model, related to Figure 2. (A) and (B) The model inference is stable against artificially added noise. (A) The parameter estimates in the models obtained with noise-added datasets are compared to the original model with the original dataset. k represents the ratio of the artificial noise SD over the residual SD of the data. Even when twice more artificial noise than the biological noise of the original data was added, the parameter estimates did not change much ($\log_2 k = 1$, dashed circle). Error bar, standard deviation. (B) The distributions of the parameter values when $\log_2 k = 1$ are shown by boxes-and-whiskers for the treatment-specific (upper panel) and the sector-specific (lower panel) parameters. Blue dot, parameter estimate in the original model. See key at top for the color-codes for the treatment and the time. (C) Treatment-specific models. The representations are the same as in Figure 2A. (D) Prediction accuracy for the held-out MAMP treatment.

Figure S4. Fragilities compared in the presence and the absence of each signaling sector, related to Figure 4. (A)-(D) the JA, ET, PAD4, and SA sectors, respectively. Dots above the $y = x$ line represent the cases where the fragility increases upon loss of the sector.

Figure S5. All network activity maps, related to Figure 5. The representations are the same as in Figure 5.

Figure S6. Effects of different factors in modeling, related to Figure 6. (A) The genotype-constrained models. The genotypes used in modeling are indicated by black dots. The heatmap shows the Jacccard index values for the sector-specific (bottom-left half) and the treatment-specific (top-right half) parameters. The bar plot shows a comparison of the parameter estimates between the "up to single" model and the original model. Red asterisk, a link that was captured only in the original full model. Error bar, 95% confidence interval. (B) The prediction accuracy of immunity levels by the constrained models. (C) The prediction accuracy of the immunity level by the genotype-constrained models. The model with the original model structure trained with the same genotype-constrained datasets and the genotype-constrained models were compared for the prediction accuracy in the values corresponding to the genotypes in the genotype-constrained datasets (top panel) or to the tripe mutant genotypes (bottom panel). Error bar, 95% confidence interval. (D) The significance of the PCC ($-\log_{10}P$) for the prediction accuracies of the sector activities with constrained models. The left heatmap is for the genotype-constrained models. The genotypes used are shown at the bottom by black dots. The right heatmap is for fewer signaling sectors in the models. The sectors included are shown at the bottom by black dots. The MAMP treatments used differ in different rows of the heatamps. The MAMP treatments used are shown at the right by black dots. The bottom heatmap is for prediction of the sector activities in the triple mutant genotypes. (E) The significance of the PCC ($-\log_{10}P$) for the prediction accuracies of the immune levels with constrained models. The representations are the same as in (D). (F) The Jaccard index values of the non-zero parameters between the constrained models and the original model. The representations are the same as in (D).

Figure S7. Network activity maps for the models with fewer signaling sectors, related to Figure 6. (A) The network activity maps for the models with three sectors. (B) The network activity maps for the models with two sectors. The representations in (A) and (B) are the same as in Figure 2A.

SUPPLEMENTARY TABLES

Table S2. Comparison of the original model and the model devoid of the inter-sector links

	The original model	The model without inter-sector links
Predictive power for sector activities	0.881	0.681
Predictive power for immunity levels	0.911	0.887

Table S3. Comparison of the invariant (original) model and the treatment-specific models

MAMP	The structure-invariant model		Treatment-specific model	
	Sector activities	Immunity levels	Sector activities	Immunity levels
flg22	0.89	0.93	0.88	0.93
elf18	0.85	0.91	0.84	0.93
chitosan	0.89	0.88	0.88	0.91

Table S4. Primers used in qRT-PCR

	Primer (5' to 3')	
At3g50280	AGCCCTTGCTTGCTTTACAA	GAAGATTCTCCCGTTGACCA

At2g41230	CTCCGAGTTTTTCTTTTCAAGG	CAATTCATAATGTGACGCTGAT
At5g46960	GAAAGACCCGCAATTGTCAT	CGTCGATGCTAGGACCAAAC
At2g14610 (*PR1)*	CGGAGCTACGCAGAACAACT	CTCGCTAACCCACATGTTCA
At4g29480	TGAAGATGGCATCGAAGTTG	TTGGCACTTCTCAACAGTGG

SUPPLEMENTAL REFERENCES

Abeles, F.B., and Rubinstein, B. (1964). Regulation of Ethylene Evolution and Leaf Abscission by Auxin. Plant Physiol *39*, 963-969.

Koller, D., and Friedman, N. (2009). Probabilistic Graphical Models: Principles and Techniques (The MIT Press).

Pieterse, C.M., Van der Does, D., Zamioudis, C., Leon-Reyes, A., and Van Wees, S.C. (2012). Hormonal modulation of plant immunity. Ann Rev Cell Dev Biol *28*, 489-521.

Siegel, S. (1956). Nonparametric Statistics for the Behavioral Sciences (New York: McGraw-Hill).

Tsuda, K., Qi, Y.P., Nguyen, L.V., Bethke, G., Tsuda, Y., Glazebrook, J., and Katagiri, F. (2012). An efficient Agrobacterium-mediated transient transformation of Arabidopsis. Plant J *69*, 713-719.

Wang, L., Tsuda, K., Sato, M., Cohen, J.D., Katagiri, F., and Glazebrook, J. (2009). Arabidopsis CaM Binding Protein CBP60g Contributes to MAMP-Induced SA Accumulation and Is Involved in Disease Resistance against Pseudomonas syringae. PLoS Pathog *5*, e1000301.

Winter, D., Vinegar, B., Nahal, H., Ammar, R., Wilson, G.V., and Provart, N.J. (2007). An "Electronic Fluorescent Pictograph" browser for exploring and analyzing large-scale biological data sets. PLoS One *2*, e718.

Wu, Z., and Irizarry, R.A. (2004). Preprocessing of oligonucleotide array data. Nature biotechnology *22*, 656-658.

Supplementary Figure 1

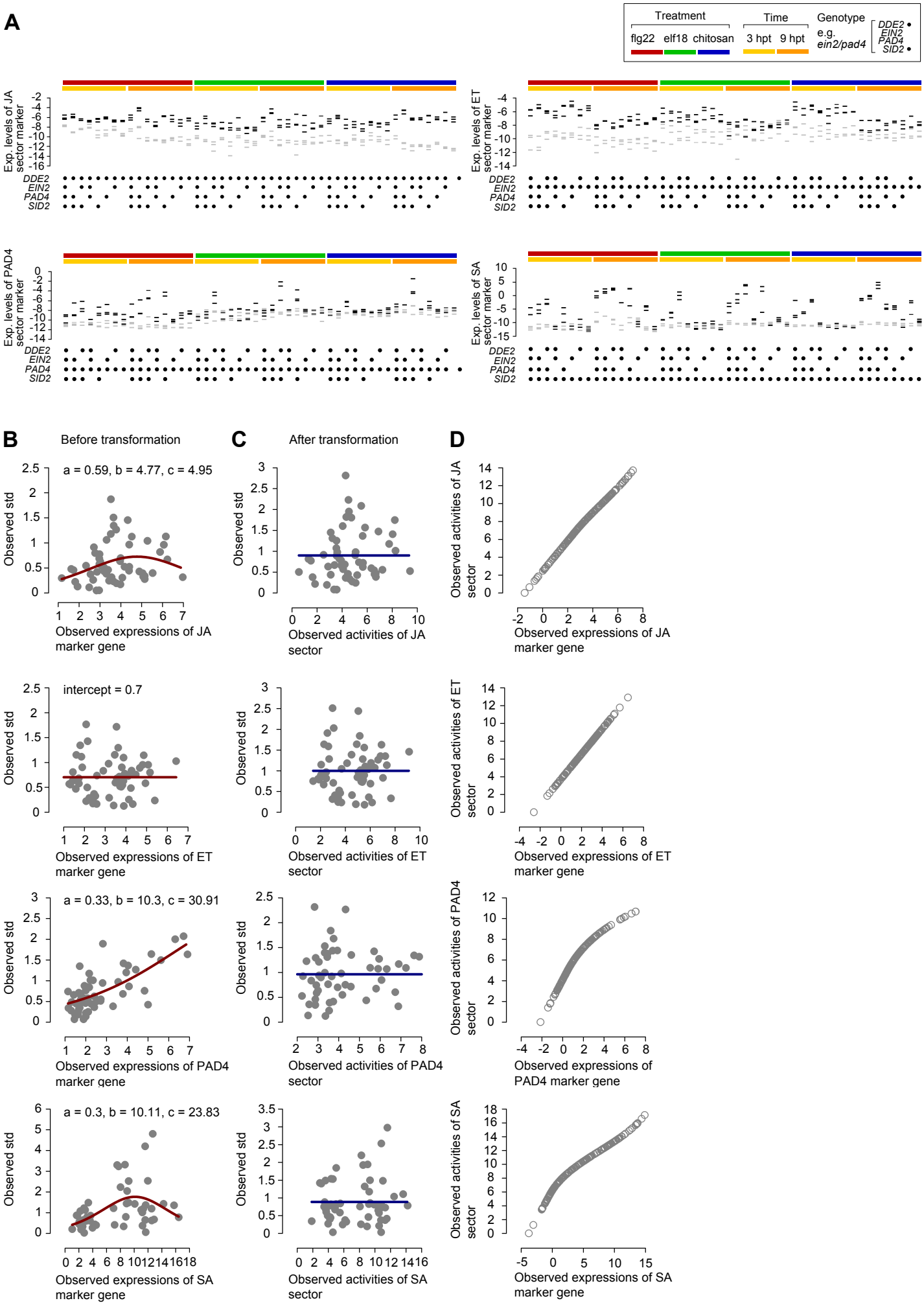

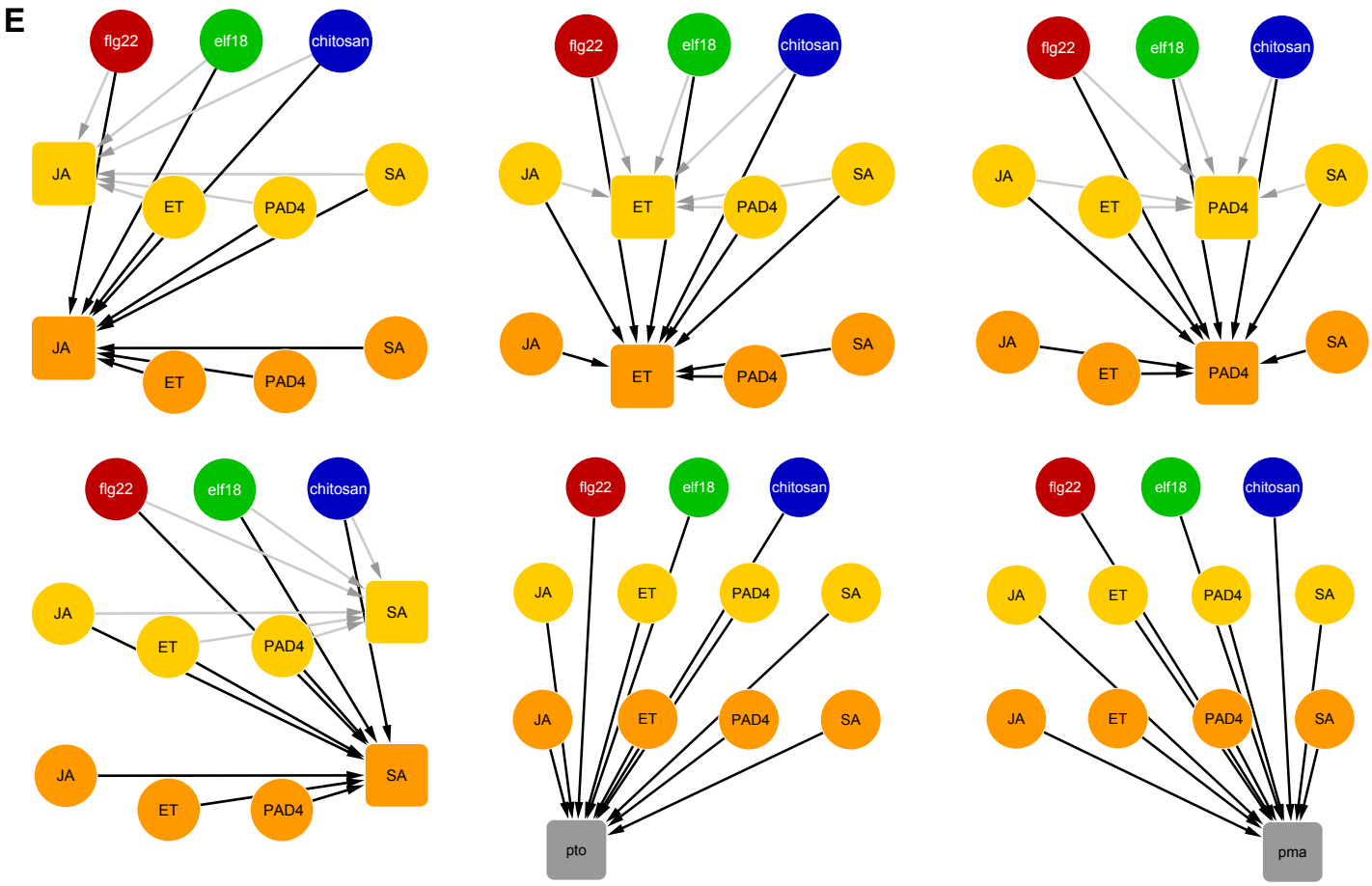
E
flg22
elf18
chitosan
JA
ET
PAD4
SA
pto
pma

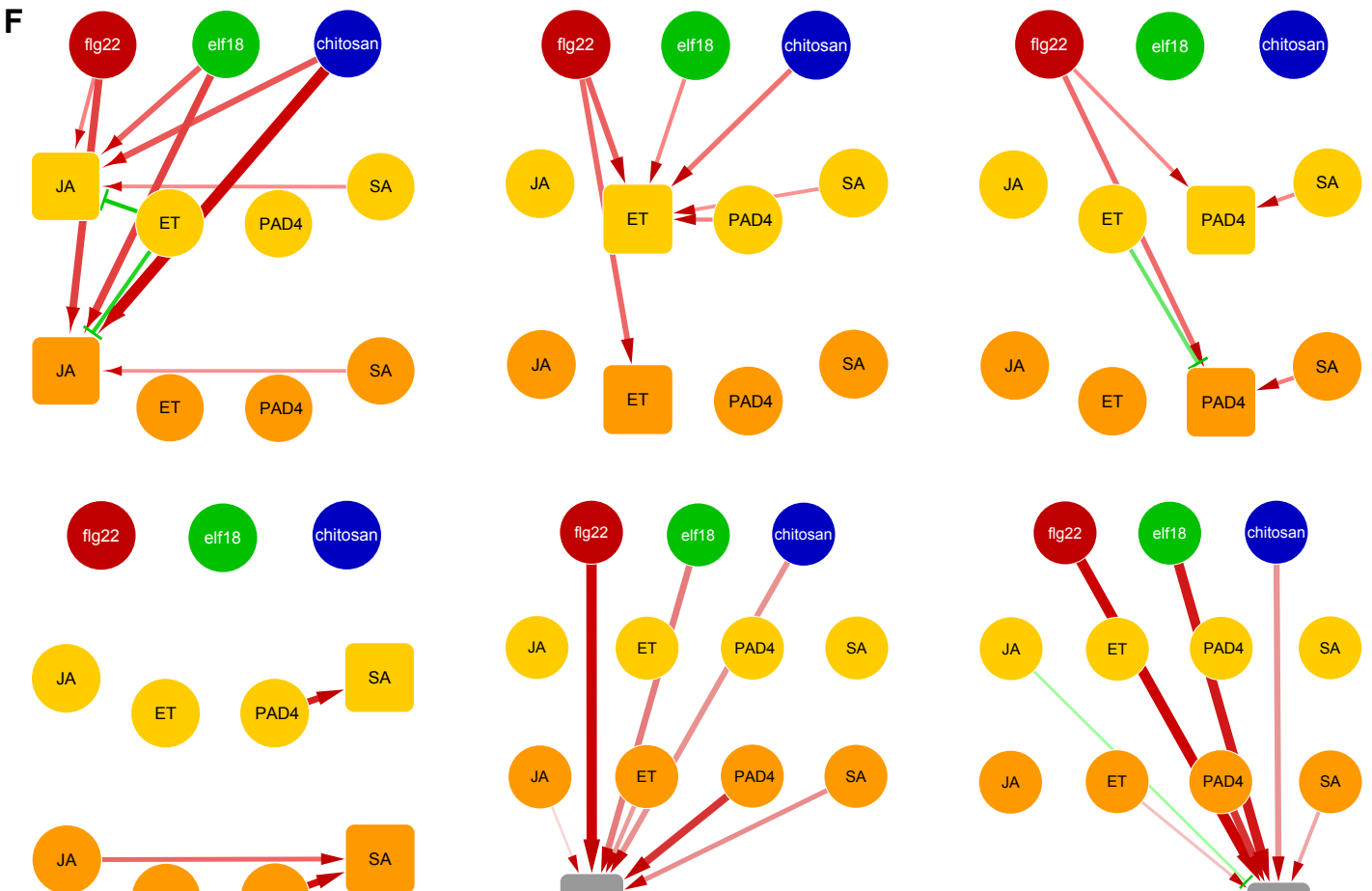
F
flg22
elf18
chitosan
JA
ET
PAD4
SA
pto
pma

Supplementary Figure 2

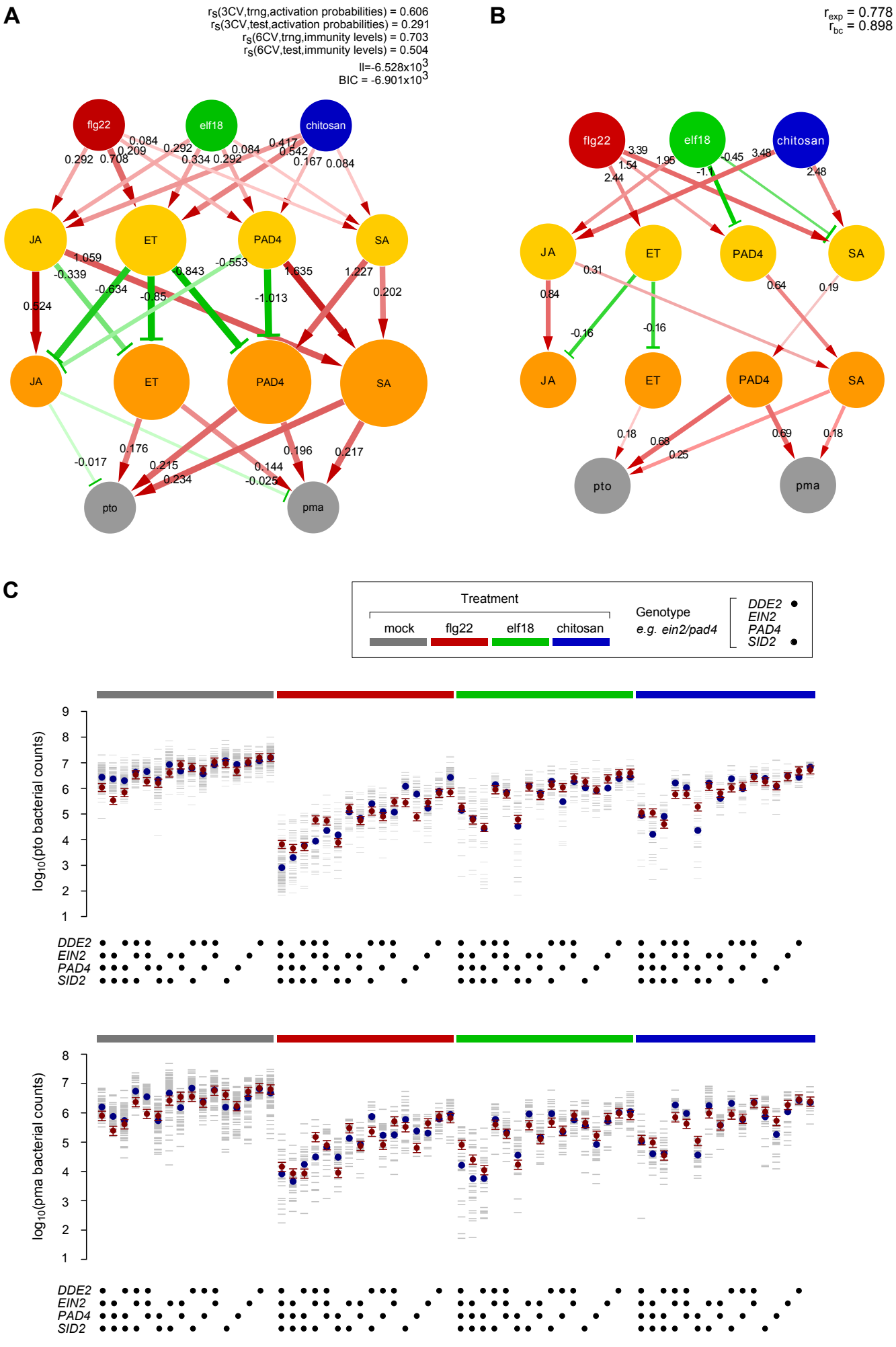

D

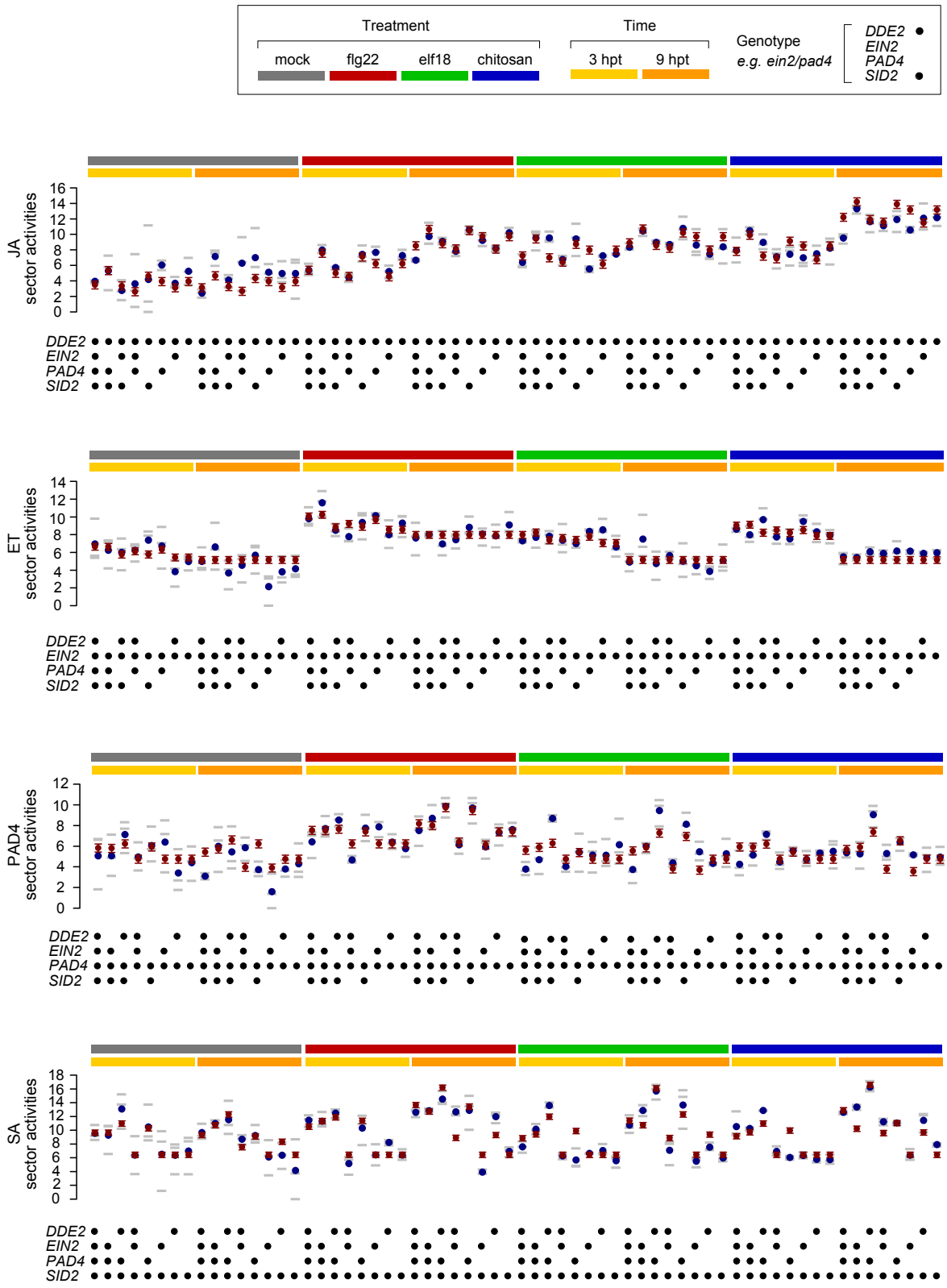
Treatment
mock
flg22
elf18
chitosan
Time
3 hpt
9 hpt
Genotype
e.g. ein2/pad4
DDE2
EIN2
PAD4
SID2
JA sector activities
ET sector activities
PAD4 sector activities
SA sector activities

Supplementary Figure 3

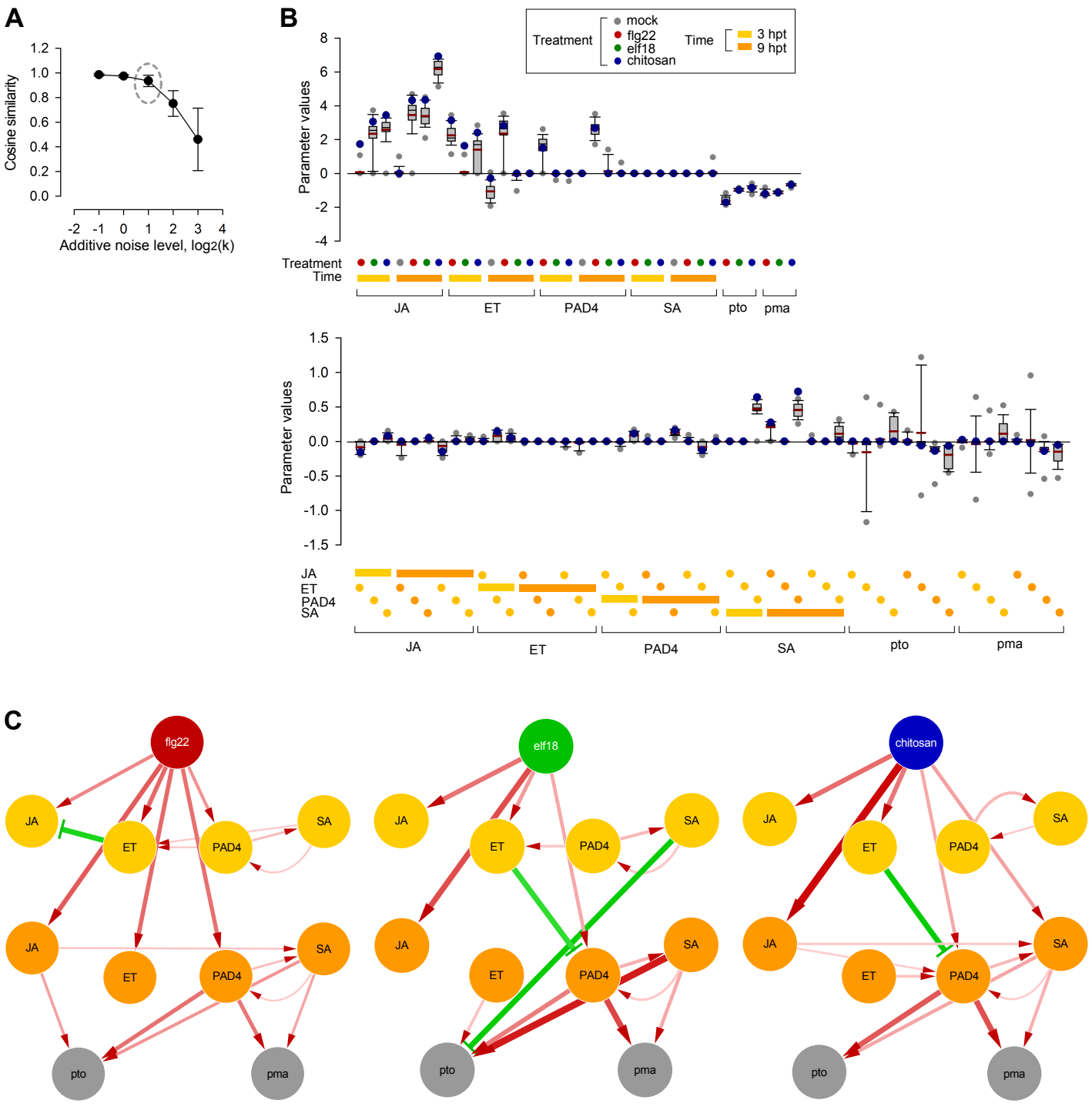

D

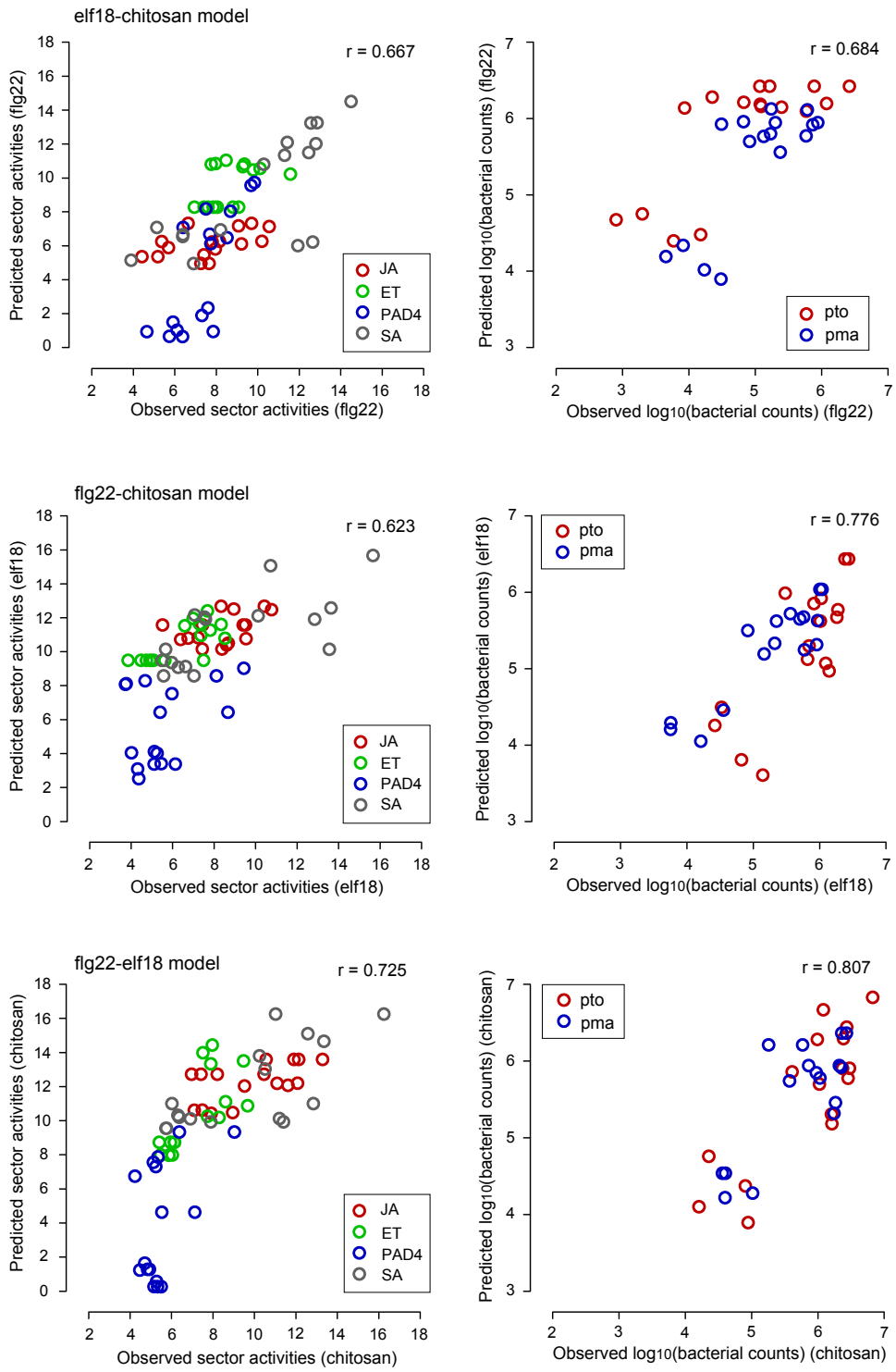
elf18-chitosan model
r = 0.667
Predicted sector activities (flg22)
Observed sector activities (flg22)
JA
ET
PAD4
SA
r = 0.684
Predicted log10(bacterial counts) (flg22)
Observed log10(bacterial counts) (flg22)
pto
pma
flg22-chitosan model
r = 0.623
Predicted sector activities (elf18)
Observed sector activities (elf18)
JA
ET
PAD4
SA
r = 0.776
Predicted log10(bacterial counts) (elf18)
Observed log10(bacterial counts) (elf18)
pto
pma
flg22-elf18 model
r = 0.725
Predicted sector activities (chitosan)
Observed sector activities (chitosan)
JA
ET
PAD4
SA
r = 0.807
Predicted log10(bacterial counts) (chitosan)
Observed log10(bacterial counts) (chitosan)
pto
pma

Supplementary Figure 4

A

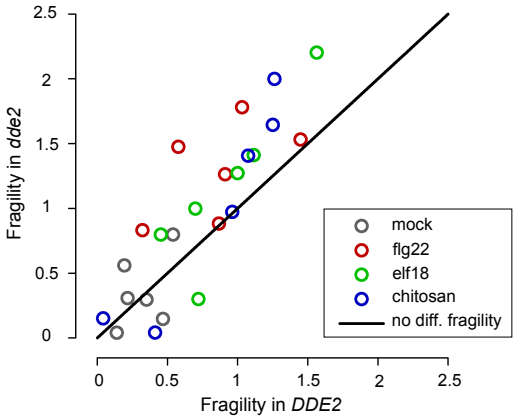

B

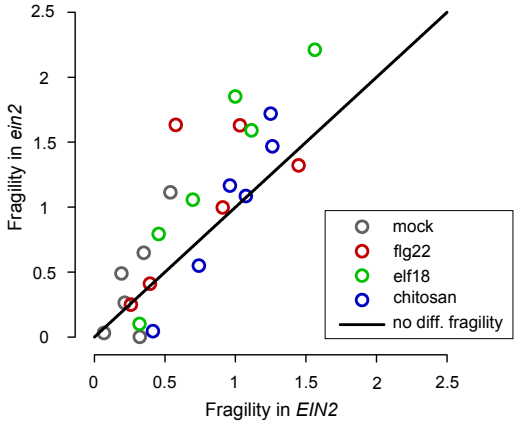

C

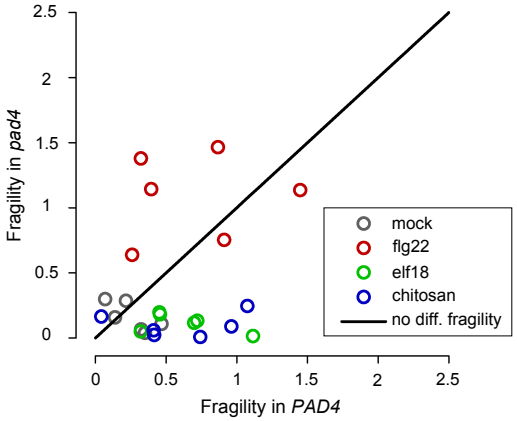

D

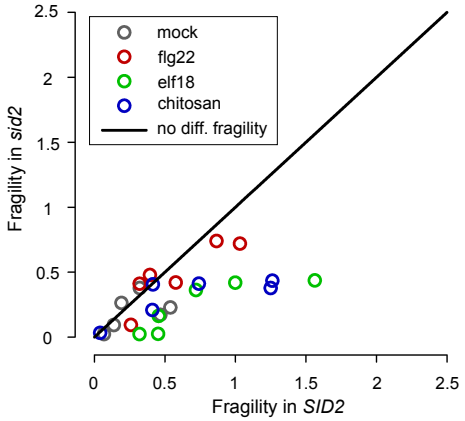

Supplementary Figure 5

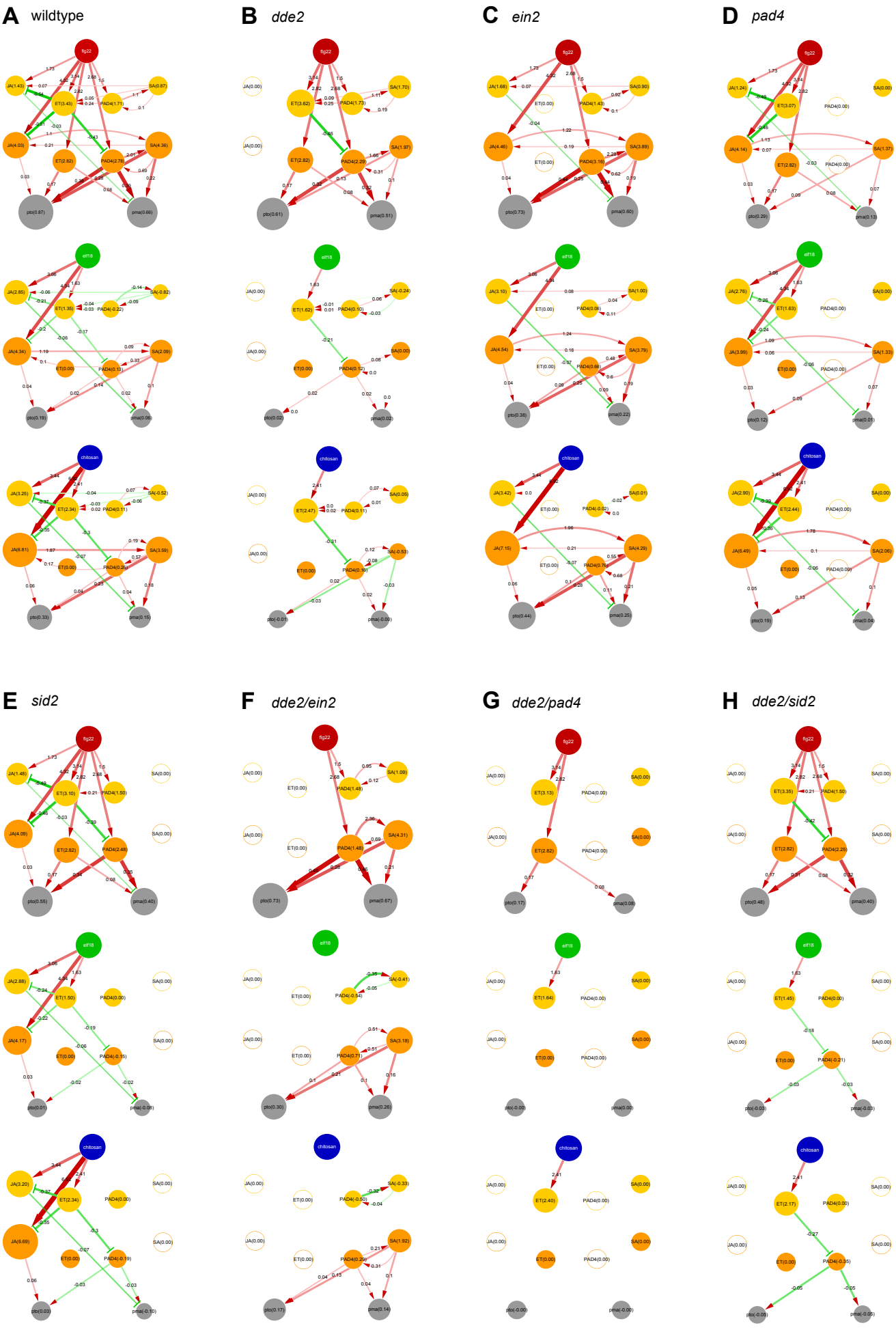

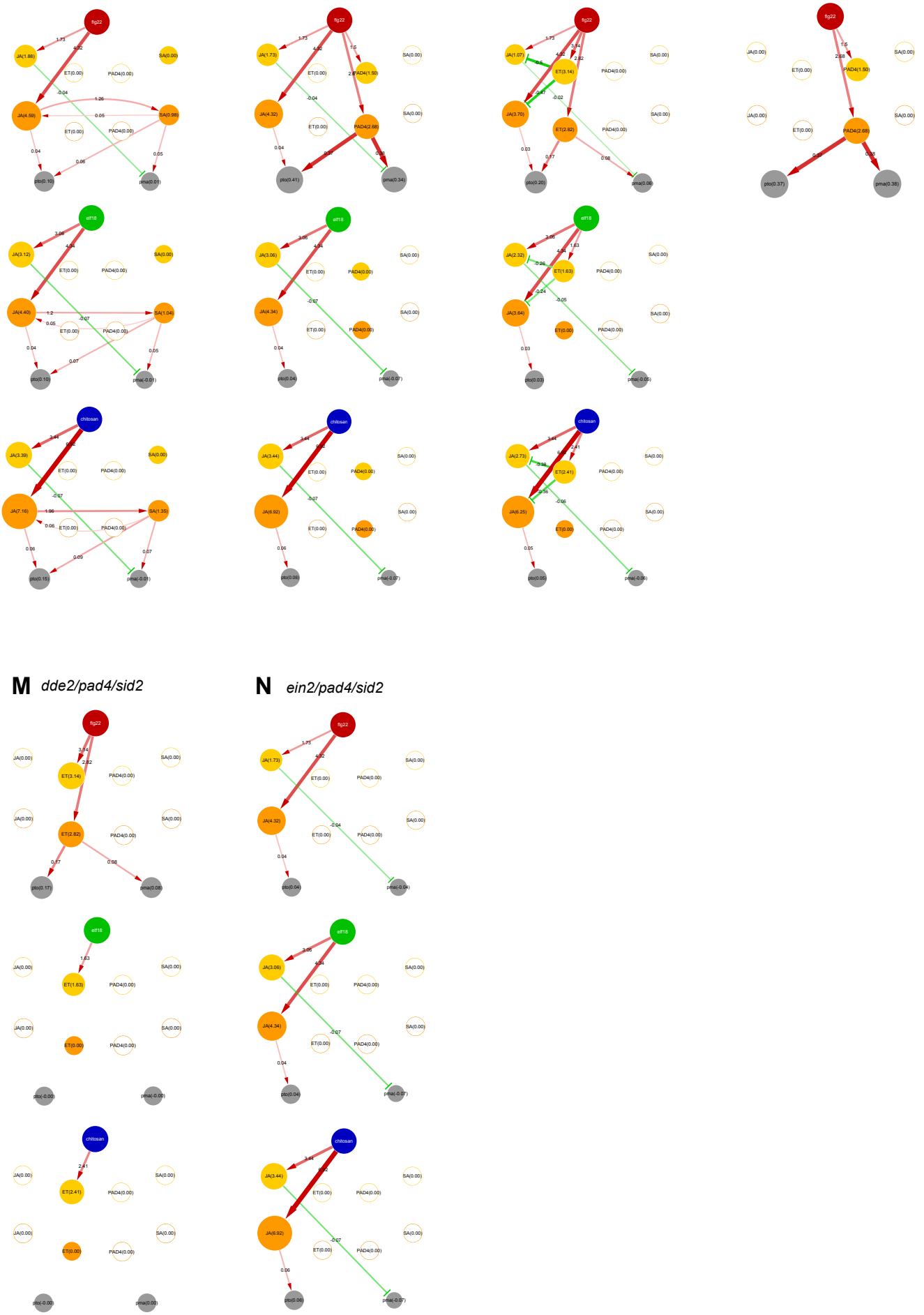
I ein2/pad4
J ein2/sid2
K pad4/sid2
L dde2/ein2/sid2
M dde2/pad4/sid2
N ein2/pad4/sid2
flg22
elf18
chitosan
JA(1.86)
JA(4.59)
SA(0.98)
JA(1.73)
JA(4.32)
PAD4(2.68)
JA(1.07)
ET(3.14)
JA(3.70)
ET(2.82)
PAD4(1.50)
JA(3.12)
JA(4.40)
SA(1.04)
JA(3.06)
JA(4.34)
JA(2.32)
ET(1.63)
JA(3.64)
JA(3.39)
JA(7.16)
SA(1.35)
JA(3.44)
JA(6.92)
JA(2.73)
ET(2.41)
JA(6.25)
ET(0.00)
PAD4(0.00)
SA(0.00)
pto(0.10)
pma(0.01)
pto(0.41)
pma(0.34)
pto(0.20)
pma(0.06)
pto(0.37)
pma(0.38)
pto(0.10)
pma(-0.01)
pto(0.04)
pma(-0.07)
pto(0.03)
pma(-0.05)
pto(0.15)
pma(-0.01)
pto(0.06)
pma(-0.07)
pto(0.05)
pma(-0.08)
pto(0.17)
pma(0.08)
ET(1.63)
pto(-0.00)
pma(-0.00)
pto(0.04)
pma(-0.04)
pto(0.06)
pma(-0.07)

Supplementary Figure 6

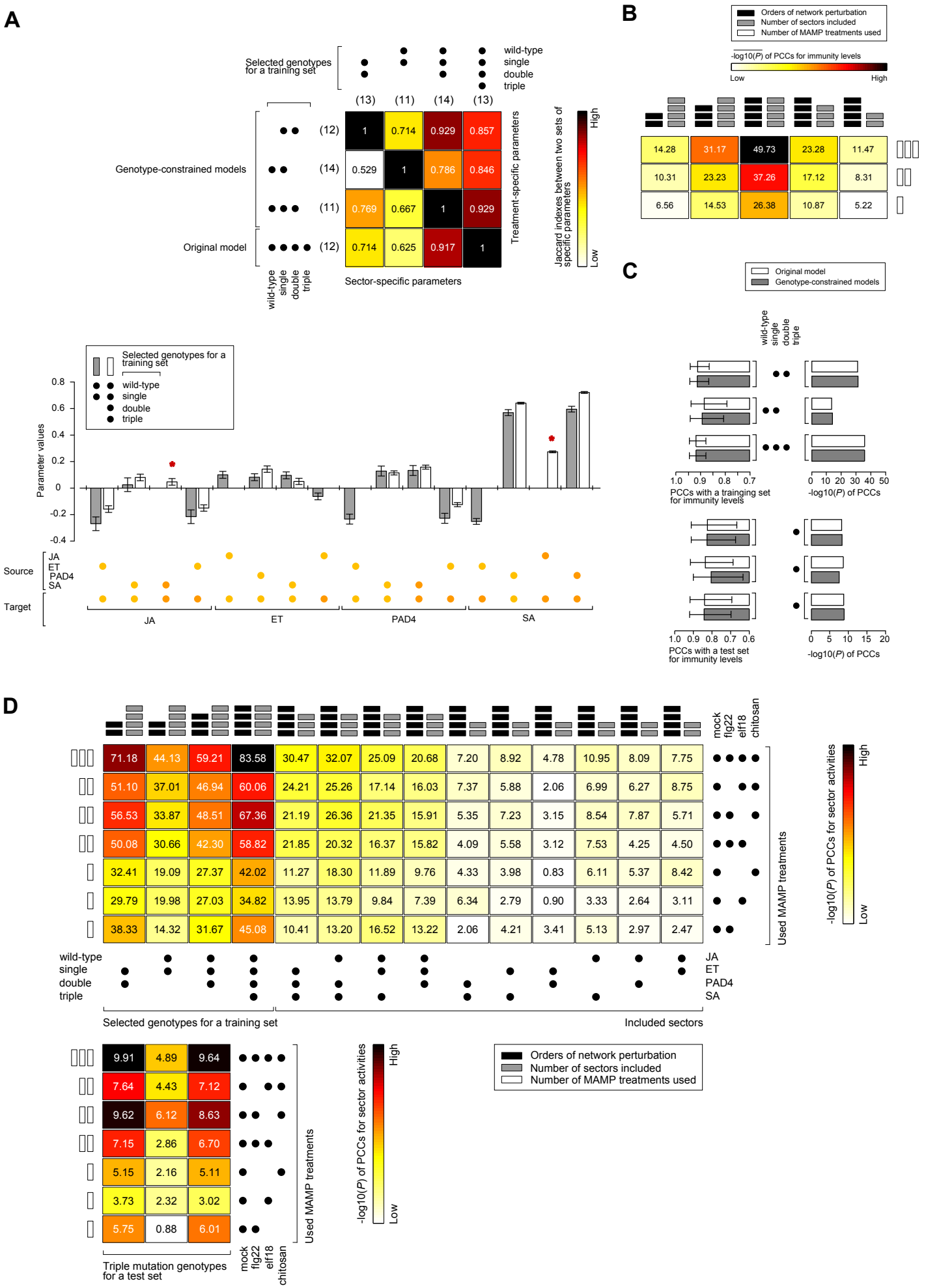

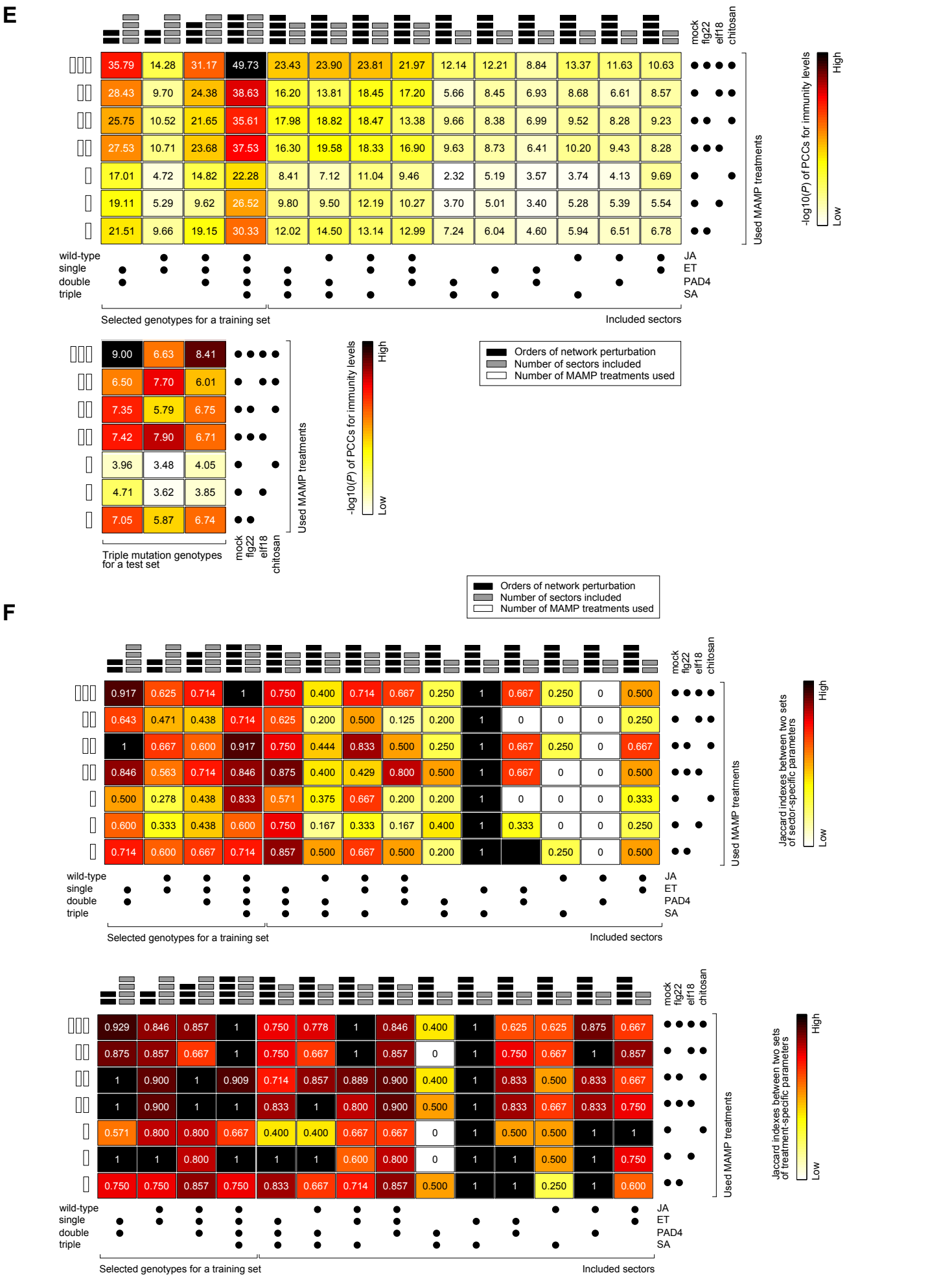
E
mock
flg22
elf18
chitosan
35.79 14.28 31.17 49.73 23.43 23.90 23.81 21.97 12.14 12.21 8.84 13.37 11.63 10.63
28.43 9.70 24.38 38.63 16.20 13.81 18.45 17.20 5.66 8.45 6.93 8.68 6.61 8.57
25.75 10.52 21.65 35.61 17.98 18.82 18.47 13.38 9.66 8.38 6.99 9.52 8.28 9.23
27.53 10.71 23.68 37.53 16.30 19.58 18.33 16.90 9.63 8.73 6.41 10.20 9.43 8.28
17.01 4.72 14.82 22.28 8.41 7.12 11.04 9.46 2.32 5.19 3.57 3.74 4.13 9.69
19.11 5.29 9.62 26.52 9.80 9.50 12.19 10.27 3.70 5.01 3.40 5.28 5.39 5.54
21.51 9.66 19.15 30.33 12.02 14.50 13.14 12.99 7.24 6.04 4.60 5.94 6.51 6.78
Used MAMP treatments
-log10(P) of PCCs for immunity levels
High
Low
wild-type
single
double
triple
JA
ET
PAD4
SA
Selected genotypes for a training set
Included sectors
9.00 6.63 8.41
6.50 7.70 6.01
7.35 5.79 6.75
7.42 7.90 6.71
3.96 3.48 4.05
4.71 3.62 3.85
7.05 5.87 6.74
Used MAMP treatments
-log10(P) of PCCs for immunity levels
High
Low
Triple mutation genotypes for a test set
mock
flg22
elf18
chitosan
Orders of network perturbation
Number of sectors included
Number of MAMP treatments used
F
Orders of network perturbation
Number of sectors included
Number of MAMP treatments used
mock
flg22
elf18
chitosan
0.917 0.625 0.714 1 0.750 0.400 0.714 0.667 0.250 1 0.667 0.250 0 0.500
0.643 0.471 0.438 0.714 0.625 0.200 0.500 0.125 0.200 1 0 0 0 0.250
1 0.667 0.600 0.917 0.750 0.444 0.833 0.500 0.250 1 0.667 0.250 0 0.667
0.846 0.563 0.714 0.846 0.875 0.400 0.429 0.800 0.500 1 0.667 0 0 0.500
0.500 0.278 0.438 0.833 0.571 0.375 0.667 0.200 0.200 1 0 0 0 0.333
0.600 0.333 0.438 0.600 0.750 0.167 0.333 0.167 0.400 1 0.333 0 0 0.250
0.714 0.600 0.667 0.714 0.857 0.500 0.667 0.500 0.200 1 0.250 0 0.500
Used MAMP treatments
Jaccard indexes between two sets of sector-specific parameters
High
Low
wild-type
single
double
triple
JA
ET
PAD4
SA
Selected genotypes for a training set
Included sectors
mock
flg22
elf18
chitosan
0.929 0.846 0.857 1 0.750 0.778 1 0.846 0.400 1 0.625 0.625 0.875 0.667
0.875 0.857 0.667 1 0.750 0.667 1 0.857 0 1 0.750 0.667 1 0.857
1 0.900 1 0.909 0.714 0.857 0.889 0.900 0.400 1 0.833 0.500 0.833 0.667
1 0.900 1 1 0.833 1 0.800 0.900 0.500 1 0.833 0.667 0.833 0.750
0.571 0.800 0.800 0.667 0.400 0.400 0.667 0.667 0 1 0.500 0.500 1 1
1 1 0.800 1 1 1 0.600 0.800 0 1 1 0.500 1 0.750
0.750 0.750 0.857 0.750 0.833 0.667 0.714 0.857 0.500 1 1 0.250 1 0.600
Used MAMP treatments
Jaccard indexes between two sets of treatment-specific parameters
High
Low
wild-type
single
double
triple
JA
ET
PAD4
SA
Selected genotypes for a training set
Included sectors

Supplementary Figure 7

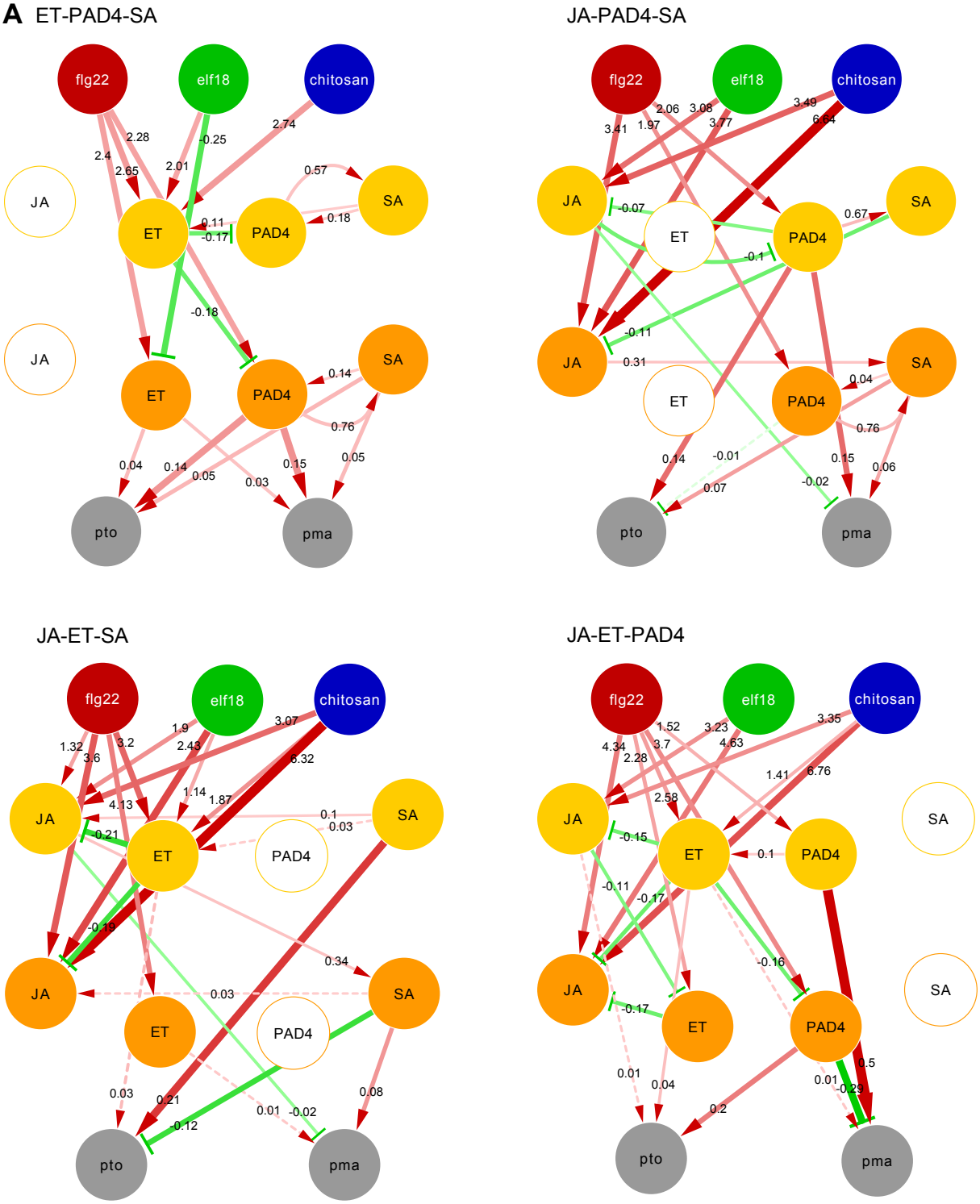

B PAD4-SA

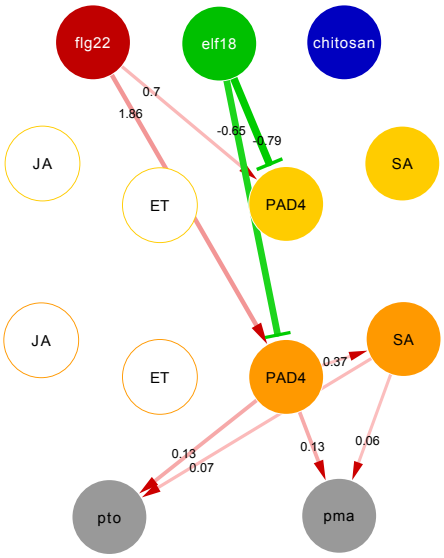

ET-SA

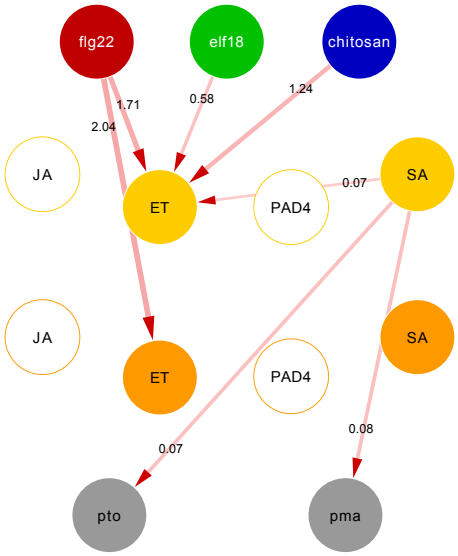

ET-PAD4

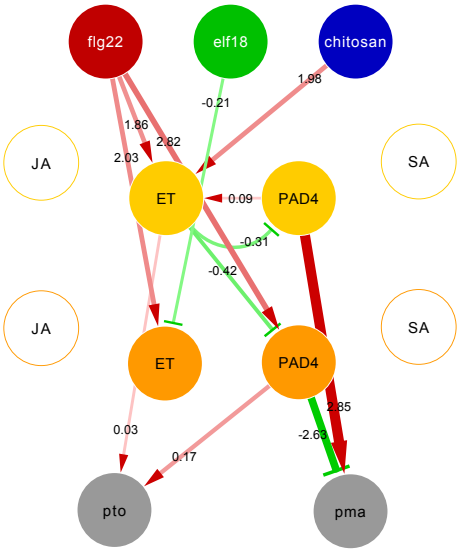

JA-SA

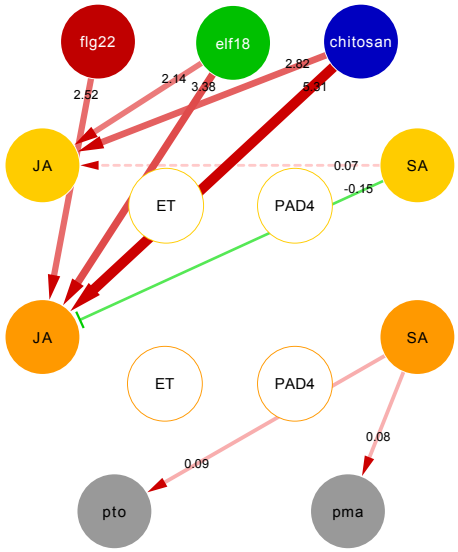

JA-PAD4

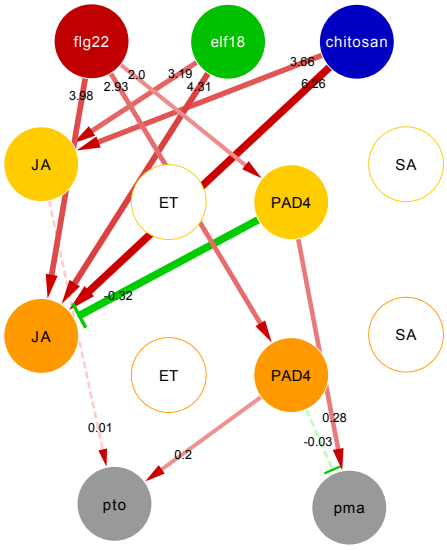

JA-ET